

FERNANDERS, MARIUM S., M.S. Crossed Molecular Beam Study of $X + O_3$ ($X = Br$ and I) and $O(^1D) + X$ ($X = Br_2, I_2, CHCl_3,$ and N_2O) Reactions via Millimeter and Sub-Millimeter Wavelength Spectroscopy. (2014)
Directed by Dr. Liam Duffy. 58 pp.

The use of scattering experiments in atmospheric studies has proved useful in understanding the dynamics of the catalytic ozone destruction cycle. By using millimeter and sub-millimeter wavelengths, we can probe bimolecular reaction systems for translational, rotational, vibrational, and electronic energy distributions through pure rotational spectroscopy. The focus of this research is on the reaction between iodine, bromine, and ozone due to their roles in the catalytic ozone destruction cycle.

For this research we studied the $X + O_3$ ($X = I$ and Br) and $O(^1D) + X$ ($X = I_2, Br_2, N_2O,$ and $CHCl_3$) reactions using single and crossed molecular beam techniques. The apparatus contains two independently rotatable arms, capable of changing collisional energies in relation to arm angle. Though no product signals have been detected at this time, critical experimental methods have been developed that can be optimized in the future.

CROSSED MOLECULAR BEAM STUDY OF THE $X + O_3$ ($X = Br$ and I) AND $O(^1D) + X$ ($X = Br_2, I_2, CHCl_3$, and N_2O) REACTIONS VIA MILLIMETER AND SUB-MILLIMETER WAVELENGTH SPECTROSCOPY

by

Marium S. Fernanders

A Thesis Submitted to
the Faculty of the Graduate School at
The University of North Carolina at Greensboro
in Partial Fulfillment
of the Requirements for the Degree
Master of Science

Greensboro
2014

Approved by

Committee Chair

APPROVAL PAGE

This thesis has written by Marium S Fernanders been approved by the following committee of the Faculty of The Graduate School at The University of North Carolina at Greensboro.

Committee Chair _____
Committee Members _____

Date of Acceptance by Committee

Date of Final Oral Examination

ACKNOWLEDGEMENTS

I would like to thank Dr. Liam Duffy for serving as my research advisor. Thank you for your patience, understanding, and guidance.

I would like to thank Dr. Alice Haddy and Dr. Solomon Bililign for agreeing to serve on my thesis committee.

TABLE OF CONTENTS

	Page
LIST OF FIGURES	vi
CHAPTER	
I. INTRODUCTION	1
I.A. Background.....	1
I.B. Catalytic Ozone Destruction Cycle via the ClO Dimer Mechanism	3
I.C. Catalytic Ozone Destruction Cycle via BrO/ClO Dimer Mechanism	7
I.D. Tucceri Iodine Experiment	9
I.E. Photodissociation of Ozone to O(¹ D).....	10
I.F. Kaucozok O(¹ D) + D ₂ Experiment	10
II. X + O ₃ REACTION	12
II.A. X + O ₃ (X= I and Br) Experimental Setup	12
II.A.1. X + O ₃ (X= I and Br) Experimental Modifications.....	16
II.B. Experimental Data for the X + O ₃ (X= I and Br) Reactions	19
II.B.1. Nitrous Oxide as Diagnostic Gas for the X + O ₃ Reaction Data.....	19
II.B.2. Experimental Data for the I + O ₃ Reaction	24
II.B.3. Experimental Data for the Br + O ₃ Reaction.....	25
II.C. Problems with X + O ₃ Experimental Modifications.....	27
II.D. Conclusions for the X + O ₃ Reactions	31
III. O(¹ D) + X REACTION	33
III.A. O(¹ D) + X Experimental Setup	33
III.A.1. Laser Optimization for the Production of O(¹ D)	39
III.B. Experimental Data for the O(¹ D) + X (X= Br ₂ , I ₂ , N ₂ O, and CHCl ₃) Reactions	42
III.B.1. Experimental Data for the O(¹ D) + Br ₂ Reaction	42
III.B.2. Experimental Data for the O(¹ D) + I ₂ Reaction	46
III.B.3. Experimental Data for the O(¹ D) + N ₂ O Reaction.....	47
III.B.4. Experimental Data for the O(¹ D) + CHCl ₃ Reaction	50
III.C. Discussion on the O(¹ D) + X Reactions.....	52
III.D. Conclusions.....	52

REFERENCES54

LIST OF FIGURES

	Page
Figure 1. Energy level diagram for the Cl + O ₃ reaction E _a = 2.08 kJ/mol.....	5
Figure 2. Energy level diagram for the Br + O ₃ reaction.....	8
Figure 3. Top down view of the X+ O ₃ chamber setup showing the rotatable arms and a projection of the molecular beams.....	13
Figure 4. Collisional energy as a function of arm angle (blue line).	14
Figure 5. Chopper blade attached to the slit nozzle, the chopper blade controls the firing sequence of the nozzles.	17
Figure 6. Relocation of the new diffusion pump, by placing the pump closer to the chamber we decreased void volume and increase vacuum efficiency.	17
Figure 7. The initial modifications to the pinhole nozzle: iodine reservoir, light detector, fiber optic holder, skimmer, temperature probe, and heater.....	18
Figure 8. Shows the placement of the light detector on the pinhole nozzle, bottom right shows detector positioned right above fiber optic opening.....	19
Figure 9. Slit nozzle mm-wave transient absorption signal of N ₂ O (N= 4 ← 3) without the chopper blade or skimmer, signal is relatively long in time (~700 μsec)	20
Figure 10. Shows the raw sequence of gas pulses pulses, in this case, pinhole and slit nozzles fired together followed by the pinhole only and then slit only.....	21
Figure 11. Shows a surface plot of the same signals in Figure 10 but with the negative going timing pulses removed.....	22
Figure 12. Shows an example of the potential avenue of data analysis.....	23
Figure 13. Scans to find the IO product signal using CMB methods	25

Figure 14. Schematic of the gas inlet manifold, the green lines represent the pathway of the argon and bromine as it goes into the pinhole nozzle for CMB experiments	26
Figure 15. 90° Push in connector and banjo fitting, the replacement of the iodine reservoir, lead to better signal from the pinhole nozzle	27
Figure 16. Signal from the pinhole using N ₂ O after replacing the iodine reservoir with 90° push in connector, secondary peak a result of N ₂ O leaking into the slit arm and out of the nozzle, due to Doppler Shift corresponding to slit nozzle location.....	28
Figure 17. Voigt profile characterized by T _{trans} = 47 K spread, 15 kHz Lorentzian broadening (gas: ozone).....	31
Figure 18. Ozone mm-wave transient absorption signal (v=0 transition)	33
Figure 19. Schematic of the laser pathway before entering the chamber	34
Figure 20. Top down view of the O(¹ D) + X experimental setup	35
Figure 21. Examples of daily diagnostic scans.....	36
Figure 22. Diagnostic scan that indicates a problem with the experiment	37
Figure 23. New set up to introduce non-gaseous reagent into the experimental chamber (located in laboratory chemical hood).....	38
Figure 24. Photodissociation OPO laser scan (over part of Hartley band) of ozone at a fixed mm-wave frequency centered on an intense ozone rotational transition (249788.5520 MHz).....	40
Figure 25. Pseudo-optimization of the pinhole, slit, and laser for CMB experiments	42
Figure 26. Sweeps for the ⁷⁹ BrO signal at the v=0 and v=1 states	44
Figure 27. Broadband frequency sweep of BrO for the v=2 state using CMB method.....	45
Figure 28. Broadband frequency sweep of BrO for the v=2 state using SMB method	46

Figure 29. Different scans to find IO signal using both CMB and SMB experimental methods	47
Figure 30. Different scans to find NO product using SMB and CMB experimental methods (all scans are $v=0$ state).....	49
Figure 31. Different scans to find ClO product using SMB and CMB experimental methods	51

CHAPTER I

INTRODUCTION

I.A. Background

Ever since the 1970's when ozone depletion was first detected, scientists have been monitoring the effects of man-made pollution and naturally occurring compounds that could affect ozone degradation. In 1995, Paul Crutzen, Mario Molina, and Frank Sherwood Rowland shared the Nobel Prize in chemistry for their work on the ozone destruction cycle. [1] Due to their efforts, it is now widely known that chlorofluorocarbons (CFCs) and brominated organic compounds have a detrimental effect on the ozone layer. The work of these laureates along with Michael McElroy's work on the BrO/ClO dimer mechanism has helped support laws and policies regarding pollution affecting the ozone layer. The most notable of these policies was the Montreal Protocol which required a gradual phase out of CFCs (and their derivatives). [2,3]

The laureates' work with CFCs showed that the photolysis of atomic chlorine, from CFCs, is responsible for 75% of the catalytic destruction of ozone. [4] When Molina and McElroy's work on the ClO and ClO/BrO dimer mechanisms in the catalytic destruction of ozone was first published, the reaction dynamics were not well understood. J.S Zhang and Y.T. Lee's crossed molecular beam (CMB) work with $X + O_3$ ($X = Cl$ and Br) reactions lead to the first breakthrough on the dynamics of ozone degradation. In our experiments, we initially attempted to study the $X + O_3$ ($X = Br$ and I) reactions due to

their similarity to the $\text{Cl} + \text{O}_3$ reaction; however, we turned to the reactions of $\text{O}(^1\text{D}) + \text{X}$ ($\text{X} = \text{Br}_2, \text{I}_2, \text{N}_2\text{O},$ and CHCl_3) after failing to detect products. The $\text{O}(^1\text{D}) + \text{X}$ reactions are more kinetically favored, while their reaction dynamics are still similar to the $\text{X} + \text{O}_3$ reactions. The goal of this research was to obtain the rovibronic (rotational, vibrational, and electronic) product state distributions of XO ($\text{X} = \text{Cl}, \text{Br}, \text{N}, \text{I}$). It is useful to study iodine containing compounds because of their relative abundance from natural and man-made sources. Natural sources of iodine tend to be concentrated in coastal regions due to oceanic algae. [5] Ever since the ban on bromomethane by the Montreal Protocol man-made iodinated compounds, specifically iodomethane, can now be found readily in pesticides. [3] Bromine containing compounds are also useful to study, ever since atomic bromine was identified as the second most abundant ozone destroying atom. Nitrous oxide (N_2O) is quickly becoming the largest stratospheric ozone depleting compound, since the Montreal Protocols ban on CFCs. [6,7] CMB experiments are useful in atmospheric studies because they can help identify or confirm the presence of transient reaction intermediates that may not be observable in normal kinetic studies. Armed with a better understanding of the reaction mechanisms, scientists and policymakers can, if necessary, develop or revise policies and laws governing the production and mitigation of ozone harming chemicals.

Crossed molecular beam experiments are essential to a detailed understanding of the dynamics of elementary chemical reactions, yielding the rotational, vibrational, translational, and electronic energy distribution of the resulting products. These distributions in turn give insight into the nature of the chemical transition state. As

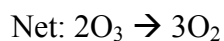
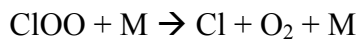
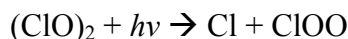
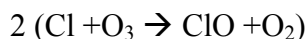
mentioned earlier, the primary focus of this research has been to obtain the rovibronic energy distributions of IO, BrO, ClO, and NO. By obtaining these distributions we can determine if the reaction has an early or late transition state geometry, and whether the reaction follows an abstraction or insertion mechanism. Prior research with the Br + O₃ reaction shows that the heavier atom reacts similar to the Cl + O₃ reaction; therefore, we expected the I + O₃ reaction ($k = 1.3 \times 10^{-12} \text{ cm}^3/\text{molecule s}$ @ 298 K) to behave similar to the widely studied Cl + O₃ reaction. [8,9,10]

While the initial goal of the thesis was to study the X + O₃ (X = Br and I) reaction, numerous experimental difficulties required us to change our experimental direction to the O(¹D) + X (X = Br₂, I₂, N₂O, CHCl₃) reaction. Despite overcoming these challenges, we failed to observe product formation in any of these reactions. We outline the possible reasons for this below.

I.B. Catalytic Ozone Destruction Cycle via the ClO Dimer Mechanism

Molina identified the ClO dimer mechanism as the catalytic pathway responsible for 75% of ozone destruction.

ClO dimer mechanism: [11,4]



Zhang and Lee carried out a dynamics experiment on the Cl + O₃ reaction to determine the angular and translational energy distributions for the ClO product in relation to the center of mass (CoM). [4] They were also able to identify the most likely geometry of the ClO₃ reaction intermediate. Zhang and Lee ran the CMB experiment at four different collisional energies (6-32 kcal/mol). Figure 1 shows the energy level diagram for the Cl + O₃ reaction. They found the translational energy was released in the forward direction with respect to the Cl atom, and the angular distribution was predominately scattered forward and sideways. [4]

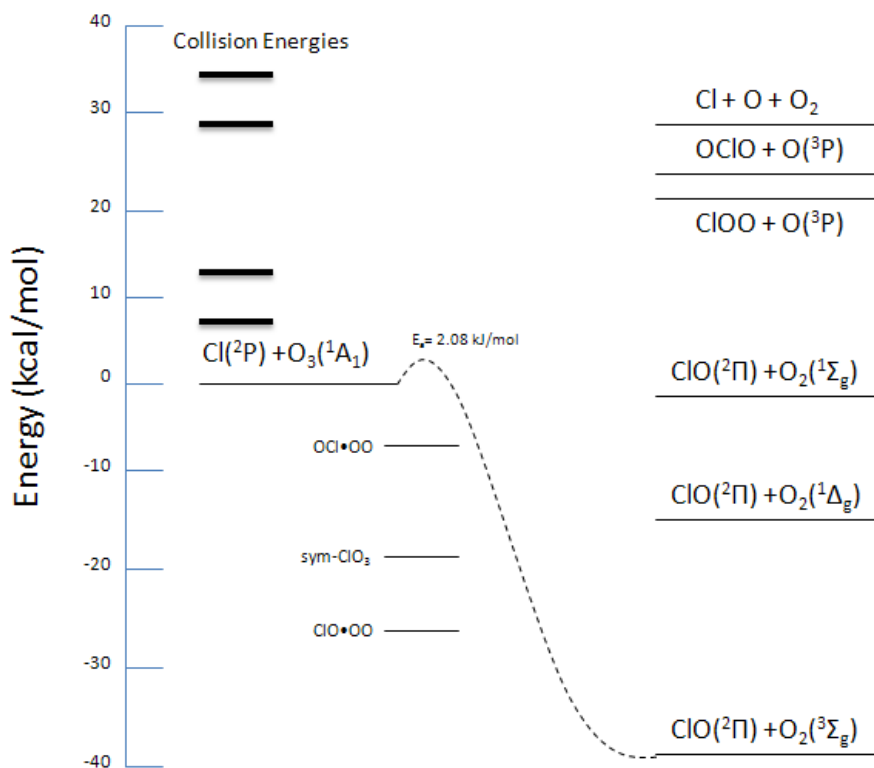


Figure 1. Energy level diagram for the Cl + O₃ reaction $E_a = 2.08$ kJ/mol. The solid black lines represent the four collision energies in the experiment. Image adapted from: Zhang, J.S.; Lee, Y.T. *J. Phy. Chem.* 101, 1997, 6485-6495.

With respect to the CoM, the translational energy ranged from 35-65% of the total collisional energy. [4] Zhang and Lee also noted that at lower collisional energies the ClO product retained more internal energy, which was a result of the Cl + O₃ reaction being largely exoergic. This was confirmed in an earlier experiment using flash photolysis on the Cl₂—O₃ reaction system. The ClO product absorption spectra showed strong absorption bands from $v=0$ to $v=5$, indicating the product comes out vibrationally excited, and primarily in the ground electronic state. [4,10]

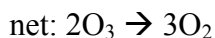
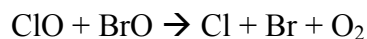
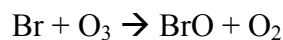
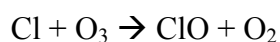
At higher collisional energies, the ClO₂ product channel becomes accessible (Figure 1). Zhang and Lee attempted to detect the ClO₂ product's two possible isomers ClOO and OCIO. The OCIO isomer is relatively stable and capable of detection through mass spectrometry (67 m/z). [4] Zhang and Lee were unable to detect signal at higher collisional energies and speculated that the OCIO product required the chlorine to undergo insertion with the ozone and, therefore, has a higher reaction barrier. The high reaction barrier makes the OCIO isomer unlikely to form in later stages of the ozone catalytic cycle.

While detection of the ClO₂ reaction channel is important, Zhang and Lee focused on the dynamics of the initial step in the ozone catalytic destruction cycle $\text{Cl} + \text{O}_3 \rightarrow \text{ClO} + \text{O}_2$. Based on the CoM angular distribution's lack of forward-back symmetry, they concluded the sym-ClO₃ and the moderately stable ClO•OO were unlikely reaction intermediates for the Cl + O₃ reaction. [4] This theory was confirmed by the lack of angular and translational energy back-scattering in the experimental data; therefore, the Cl + O₃ reaction is consistent with a direct reaction with no long-lived intermediates. [9]

I.C. Catalytic Ozone Destruction Cycle via the BrO/ClO Dimer Mechanism

The ClO/BrO mechanism identified by McElroy is the second most significant cause of catalytic ozone destruction. The Br + O₃ reaction is a key initial step in the ClO/BrO mechanism.

ClO/BrO mechanism: [4,12]



Zhang and co-workers studied the Br + O₃ reaction in order to compare it to previously published dynamics data on the Cl + O₃ reaction. Based on prior kinetic studies on X + O₃ reactions (X= O(³P), F, Cl, and Br) the pre-exponential factors were all similar (~2.2 X 10⁻¹¹ cm³ molecule⁻¹s⁻¹). [4] As a result, the Br + O₃ reaction is expected to behave similar to the Cl + O₃ reaction.

Zhang et al. ran their experiment at five different collisional energies (5-26 kcal/mol) to obtain the translational energy and angular distributions for comparison to the Cl + O₃ reaction. Figure 2 shows the energy level diagram for the Br + O₃ reaction. [13]

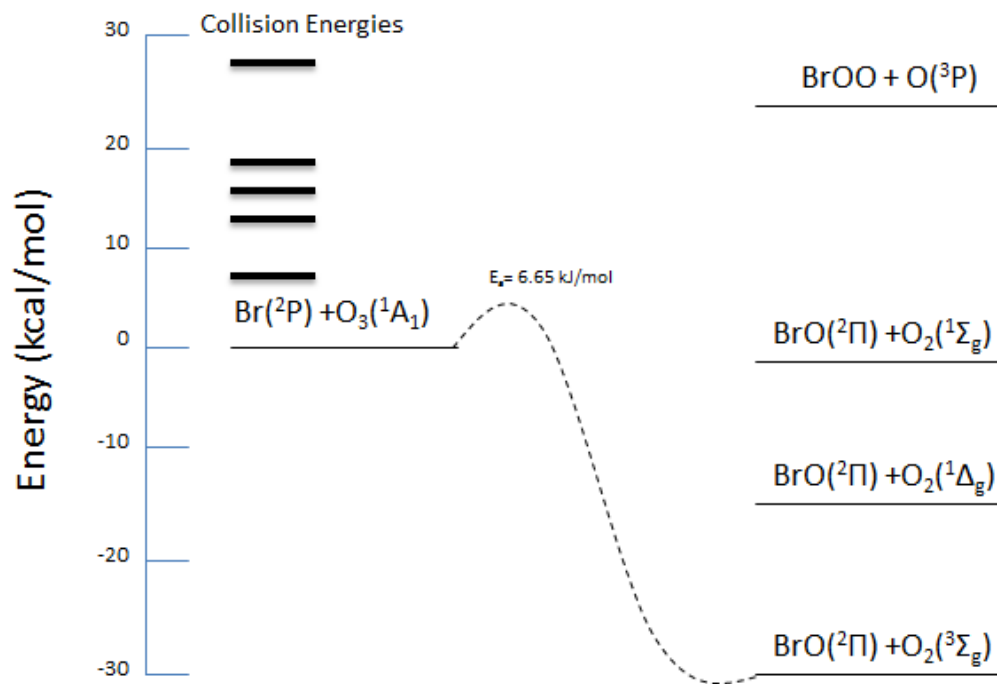


Figure 2. Energy level diagram for the Br + O₃ reaction. The solid black lines represent the five collision energies (5-26 kcal/mol) in the experiment. Image adapted from: Zhang, J.S.; Lee, Y.T. *J. Phy. Chem.* 101, 1997, 6922-6930.

There are three possible products of the Br + O₃ reaction: ground state O₂ and two excited state O₂ molecules. At higher collisional energies, the semi-stable BrO₂ intermediate pathway opens up. Zhang and coworkers attempted to detect the BrO₂ intermediate, but were unable to. They speculated that this was due to the relatively weak Br—O₂ bond (~1 kcal/mol) that could be broken during the ionization process. Or more likely, the Br + O₃ reaction does not contain an intermediate reaction channel. [13] This was confirmed by the lack of forward-back scattering in the experiment. They found the translational energy was forward scattered with respect to the CoM, and the angular distribution was forward and side scattered.

I.D. Tucceri Iodine Experiment

Iodomethane (CH₃I) has recently become of interest in atmospheric chemistry as a potential reagent in the ozone catalytic destruction cycle, but there has been very little experimental data on the reaction dynamics or kinetics of the I + O₃ reaction. [14]

Tucceri and coworkers used laser flash photolysis coupled with resonance-fluorescence to measure the rate coefficients for the I + O₃ reaction. [15] They found that atomic iodine's decay is defined by: [15]

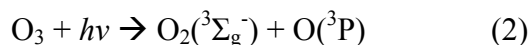
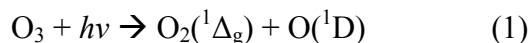
$$[I]_t = [I]_0 e^{-k'_1 t} \quad (1.1)$$

$$\text{Where } k'_1 = k_1 [O_3] + d \quad (1.2)$$

Here, d represents the loss of reagent through diffusion or side reactions. For their experiment, N₂O acts as a scavenger reagent to minimize and/or prevent any side reactions, since the IO product tends to undergo self-reactions, which can artificially inflate the unreacted atomic iodine in the experiment. [15] Tucceri et al. increased the concentration of atomic iodine at a constant ozone concentration and recorded no significant change in the production of product (IO). By taking the slope of k'_1 vs [O₃], they were able to obtain k_1 of the reaction $(1.28 \pm 0.06) \times 10^{-12} \text{ cm}^3 \text{ molecule}^{-1} \text{ s}^{-1}$. Their data corresponds with previous research by Holscher and coworkers $(1.2 \pm 0.1) \times 10^{-12} \text{ cm}^3 \text{ molecule}^{-1} \text{ s}^{-1}$. [16,15]

I.E. Photodissociation of Ozone to O(¹D)

The photodissociation of ozone is a naturally occurring reaction in the stratosphere. It is due to ozone's ability to photodissociate at ultraviolet (UV) wavelengths that protects the earth's surface from harmful UV radiation. Peak ozone absorption occurs in two areas of the UV spectrum the Hartley band (220-310 nm) and Huggins band (310-360 nm). [17,18] When undergoing photodissociation, ozone can follow two separate reaction channels: [17]



With the dominant reaction channel dependent on what wavelength of light ozone absorbs. The Hartley band is one of the primary sources of O(¹D) production, with peak O(¹D) synthesis occurring at wavelengths less than 300 nm. [19,20]

I.F. Kauczok O(¹D) + D₂ Experiment

Kauczok et. al. ran a PHOTOLOC single molecular beam experiment for the O(¹D) + D₂ reaction. The scientist produced O(¹D) atoms through hole burning, by photodissociating N₂O molecules with a laser set to 193 nm. They then used a rotatable Time-of-Flight Mass Spectrometer (TOF-MS) to measure the D atoms that resulted from the O(¹D) + D₂ reaction. [21]

From this the scientist found that the O(¹D) + D₂ reaction was predominantly back-scattered with respect to the D₂ molecule. The back-scattering of the D atom is

consistent with an insertion mechanism. They also found that the product came out primarily in the $v=4$ and 5 state. [21,9,4]

CHAPTER II

X + O₃ REACTION

II.A. X + O₃ (X= I and Br) Experimental Setup

The crossed molecular beam experiment is relatively new to the Duffy research group. In previous years, Duffy's lab worked on single molecular beam experiments using lasers. The previous graduate students: Jouse Monge, Daniel Mauney, and Nicholas Mark modified the group's prior setup to run CMB experiments. [22,24,26] The focus of their research was on different forms of CMB scattering and the theoretical approach of CMB data analysis through Fourier Transform Doppler Spectroscopy (FTDS). [22,23] Mark's efforts with atomic chlorine and ozone served as the catalyst for our experiment with X + O₃ (X= Br and I) and O(¹D) + X (X= I₂, Br₂, N₂O, and CHCl₃). Nicholas Mark conducted experiments in which he attempted to generate atomic chlorine by the use of electrical discharge. Unfortunately, his method generated significant RF noise, interfering with the data acquisition electronics, as well as the operation of the gas pulse nozzles. The need for high voltage and high current fast switches was also problematic. [24,25]

Figure 3 shows a top-down view of the experimental setup. The lower figure shows a projection of the molecular and microwave beams. Once a given collisional energy is chosen by adjusting the relative angle between the arms, the arms may then be moved in tandem to allow the products to be probed by means of Doppler spectroscopy.

By moving the arms, over a range of angles, the full 3D velocity distribution of the products may be determined by FTDS. In the chamber the nozzle arms can be set at a range of angles from 45° to 180° apart, allowing the initial relative kinetic energy of the reactants to vary (Figure 4). In this case, FTDS will be used to determine the angular distributions of the overall reaction $X + O_3$ ($X = \text{Br}$ and I). We hoped to use these distributions to gain insight into the transition state geometries, reaction intermediates, and basic mechanisms.

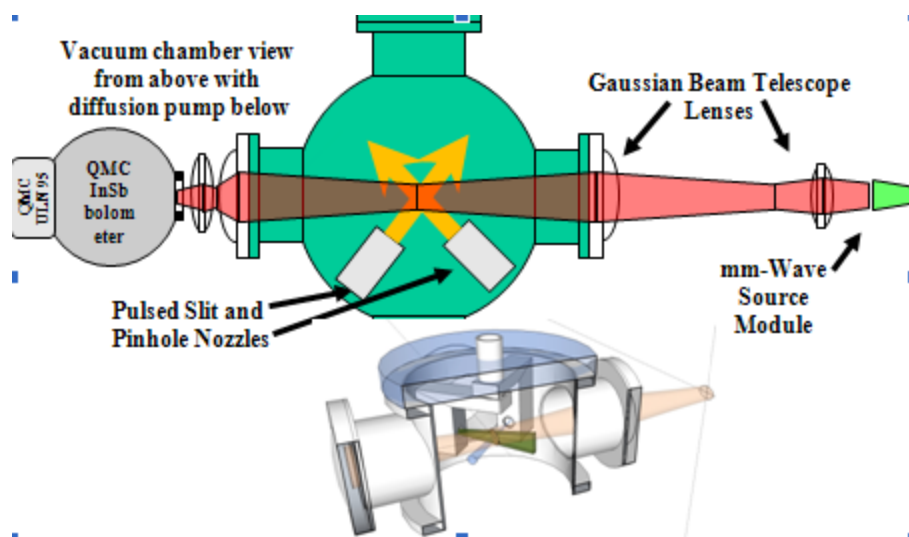


Figure 3. Top down view of the $X + O_3$ chamber setup, showing the rotatable arms and a projection of the molecular beams.

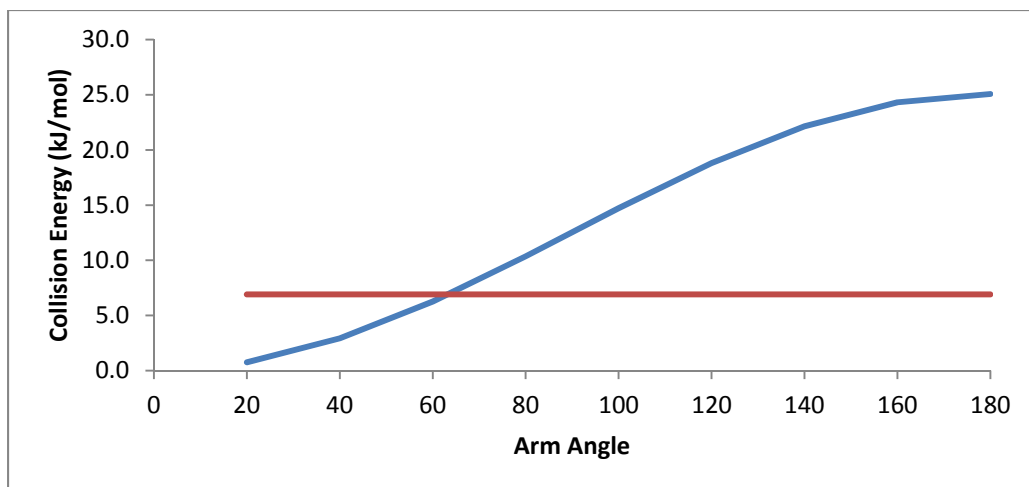


Figure 4. Collisional energy as a function of arm angle (blue line). Reported activation energy, of 6.9 kJ/ mol @ 300 K (red line), for the I + O₃ reaction.

Because molecular bromine does not have a millimeter wave spectrum, we tested our system timing using acetonitrile before each experimental run. A vial of acetonitrile was attached to the gas inlet system (the bromine was set up in the same way) and argon gas was passed through the liquid. The microwave frequency was set to a rotational state of acetonitrile, and a test scan was taken. When we were satisfied with the timing, the iodine/bromine ozone experiment was initiated.

Ozone was fired through the slit nozzle with argon acting as the carrier gas. Atomic iodine was generated at the pinhole nozzle exit from the dissociation of molecular iodine by using a continuous wave (CW) line tunable Ar/Kr laser set at 488 nm. Again, argon was used as the carrier gas. The pressure of each nozzle was monitored individually using the gas inlet system. An optical sensor spanning across the chopper blade, and mounted on the arm of the slit nozzle, was used as a trigger for the nozzle

firing. A custom-made timing circuit was used to synchronize the chopper and slit gas pulse firing, as described in the thesis of Daniel Mauney. [26] The microwave frequency was set to a rotational state of the product molecules (IO and BrO).

Ozone was created, in the laboratory fume hood, with a commercially available generator (Pacific Ozone G 11) in accordance with the owner's manual. Neat O₂ was passed through the generator at a 10% flow rate of total possible gas flow. The ozone output was set at 70% and the generator was run for a minimum of thirty minutes. The ozone was then captured on silica beads cooled in a dry ice/ acetone bath (-78 °C) allowing the unreacted waste stream of O₂ to pass through the beads. As a precaution, any trace ozone that may have passed through the silica was diminished in a heated 4" diameter pipe containing copper wool at 100°C and then exhausted into the chemical hood. [27] We knew we had obtained ozone when the silica beads had taken on a dark blue/ purple hue. To facilitate the flow of ozone to the cross molecular beam apparatus, argon was passed over the trapped ozone. It is also important to note, that mixtures of ozone and molecular oxygen are potentially explosive, as is neat ozone liquid undergoing evaporation. Researchers intending to work with or trap ozone should read the references cited here. [28,29] We have not had any problems working with pure neat ozone evaporating from silica gel held at -78 °C and carried to the experiment via ¼" Teflon tubing. It is critical that liquid nitrogen not be used to trap ozone as this would lead to the capture of molecular oxygen on the beads and possible explosion. [28,29]

Iodine crystals were placed in a reservoir attached to the pinhole nozzle (Figure 8). The crystals were heated to increase their vapor pressure and argon was used as a

carrier gas. We estimated the molecular iodine concentration within the molecular beam using baratron pressure sensors attached to the gas inlet system. Due to the relatively weak nature of the I_2 (151 kJ/mol) bond, we chose to make atomic iodine by photolysis using a laser (Melles Griot 43 ion series) tuned to approximately 488 nm.

Molecular bromine was introduced to the chamber via a vial attached to the gas inlet system. Argon gas was passed through the liquid bromine to facilitate evaporation. The bromine vapor came out the pinhole nozzle where we photodissociated the molecular bromine using a laser (Melles Griot 43 ion series) tuned to approximately 510 nm. [30] We confirmed the presence of atomic bromine with the Spectra International Residual Gas Analyzer Mass Spectrometer (RGA) by pulsing bromine vapor into the chamber with the laser on.

II.A.1. $X + O_3$ (X= I and Br) Experimental Modifications

To optimize the cross molecular beam apparatus for the $X + O_3$ (X= I and Br) experiments, we made several modifications to the chamber. One such modification was the addition of skimmers to the pinhole and slit nozzles. The skimmers decreased the molecular spread of the pulsed gas, which in turn narrowed the Doppler line width.

As mentioned earlier, in some experiments a chopper blade was added downstream from the slit nozzle in order to shortening the gas pulse, and in conjunction with an optical sensor, act as a timing mechanism (Figure 5). During the initial testing of the chopper blade, we experienced problems with the motor. After consultation with the company engineers, we suspected the chopper motor was overheating. To prevent this,

we replaced the original dc motor (Maxon Amax 16 motor) with a larger one (Maxon Amax 26 motor) and added a temperature probe to decrease the risk of overheating while under vacuum (Figure 5).

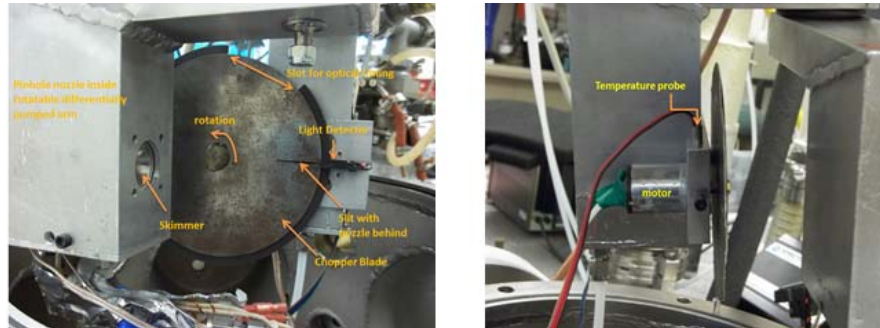


Figure 5. Chopper blade attached to the slit nozzle, the chopper blade controls the firing sequence of the nozzles. Side view of the chopper shows the installation of the larger motor and temperature probe.

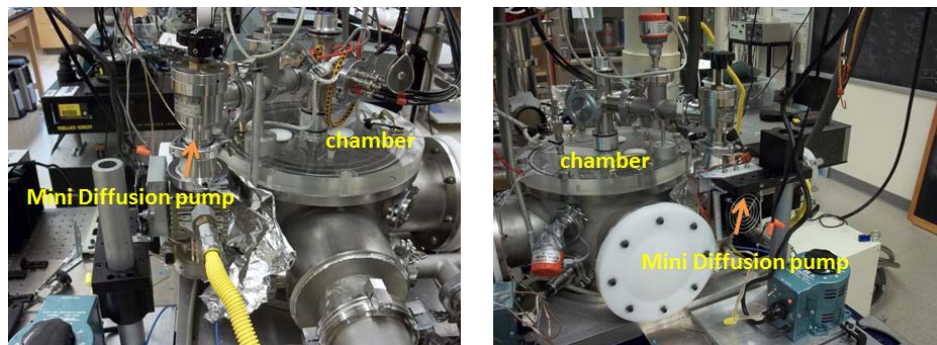


Figure 6. Relocation of the new diffusion pump, by placing the pump closer to the chamber we decreased void volume and increase vacuum efficiency.

Since the nozzles were firing within quick succession of each other, there was a possibility of overwhelming the vacuum system. To combat the problem, we relocated and replaced the mini diffusion pump (air-cooled Edwards E050/60 pump, Figure 6). By

moving the diffusion pump closer to the chamber we had decreased void volume, increased pumping efficiency, and decreased pump down time.

In order to use a laser to generate atomic iodine, we made extensive modifications to the pinhole nozzle holder (Figure 7). These include a fiber optic cable holder, a light detector (Figure 8), an iodine reservoir/heater holder, and a temperature probe. Because the entire nozzle was enclosed, we added a photoresistor light detector to indicate if the laser was on. Signal intensity could be monitored with a voltmeter, where a 9 V reading indicated the laser was off and a 0 V reading indicated full power.

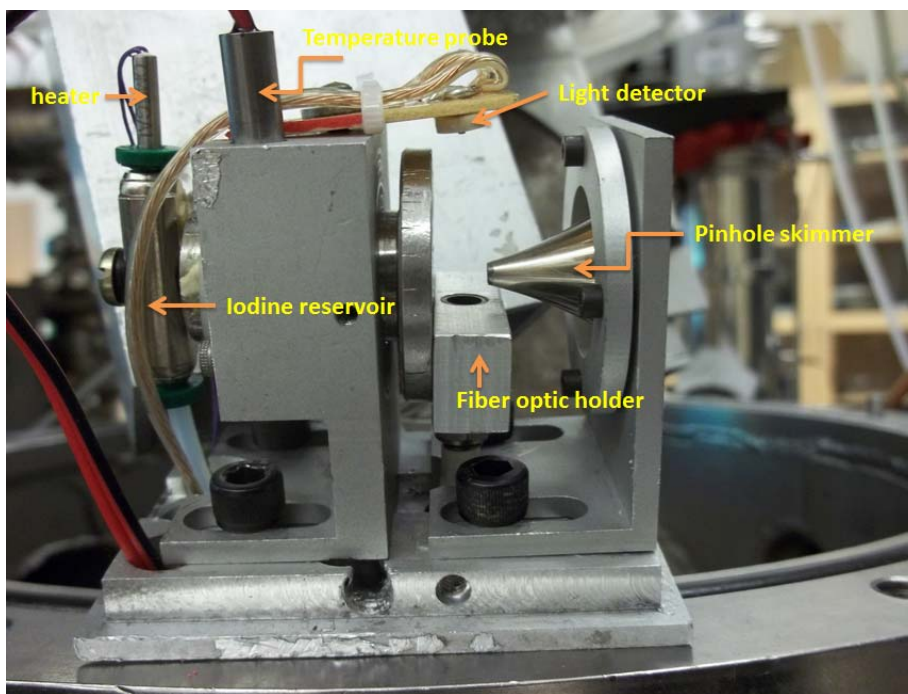


Figure 7. The initial modifications to the pinhole nozzle: iodine reservoir, light detector, fiber optic holder, skimmer, temperature probe, and heater

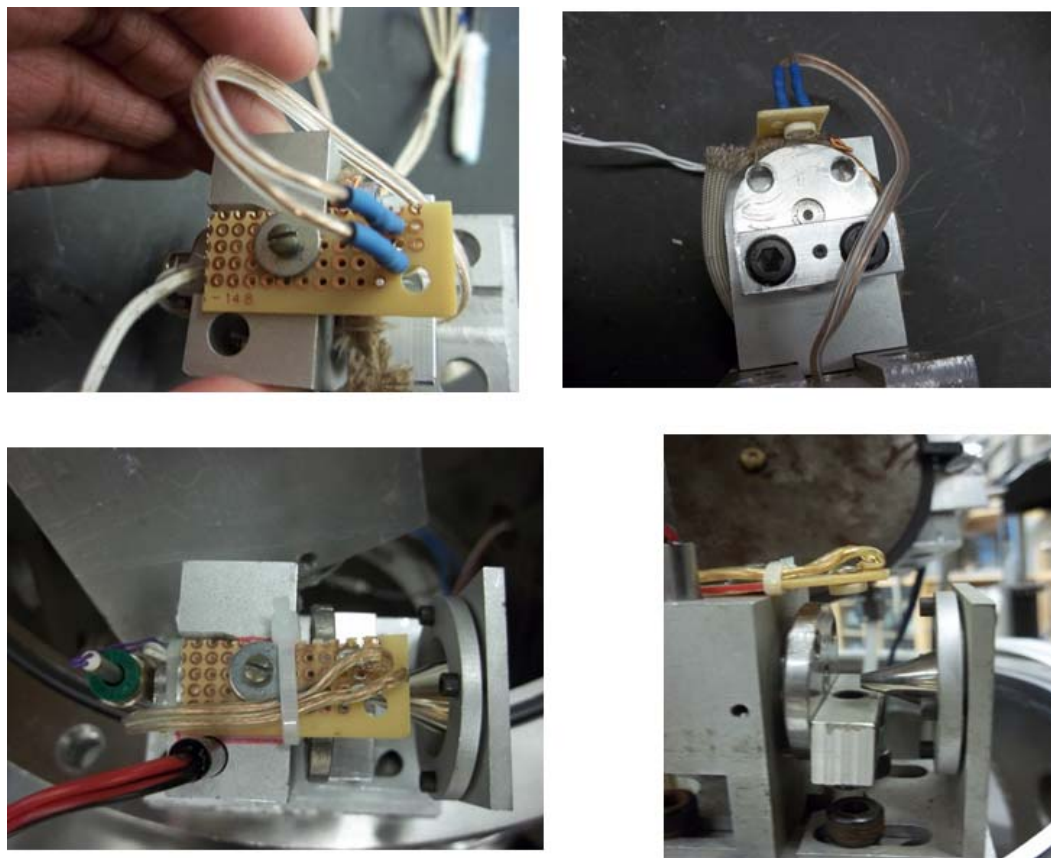


Figure 8. Shows the placement of the light detector on the pinhole nozzle, bottom right shows detector positioned right above fiber optic opening.

II.B. Experimental Data for the $X + O_3$ ($X= I$ and Br) Reactions

II.B.1. Nitrous Oxide as Diagnostic Gas for the $X + O_3$ Reaction Data

Due to the low cost, toxicity, and relatively simple spectra of nitrous oxide (N_2O), we used it as one of our diagnostic gases for the modifications to the chamber and data acquisition program. The data acquisition program plots a 3D representation of the signal absorption intensity as % Absorbance vs. Frequency (MHz) and Time (μ secs). Figure 9 shows a single rotational line of N_2O , without the chopper (left) as well as a rotational

line of N_2O with the addition of the skimmer and chopper (right). By adding the skimmer and chopper, we narrowed the signal in time.

To reduce errors associated with systematic drifts in pressure and other parameters, we modified the data acquisition so all three signals (pinhole, slit, and both) are collected sequentially and graphed during the same run (Figure 10-11). We were also able to identify which nozzle corresponds to which peak via Doppler shift and the time scale each nozzle fires on. In Figure 9 the signal shifted to a lower frequency from line center, which indicated the molecules are moving towards the mm-wave source. In this case, the signal is from the slit nozzle, which is oriented 45° from the mm-wave axis. Each gas nozzle trigger signal is a different length, which we used to identify the order of the nozzle firing sequence (Figure 10-11).

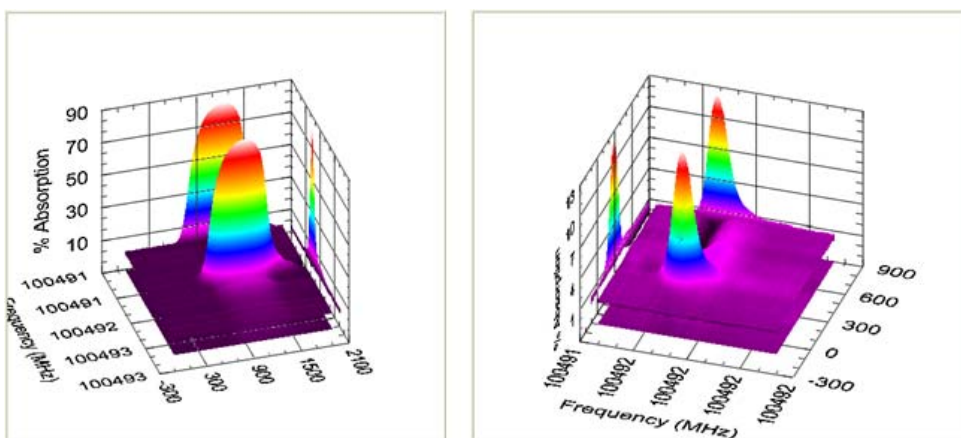


Figure 9. Slit nozzle mm-wave transient absorption signal of N_2O ($N=4 \leftarrow 3$) without the chopper blade or skimmer, signal is relatively long in time ($\sim 700 \mu\text{sec}$). Left figure shows the same N_2O transition as the right but with skimmer and chopper blade attached, signal becomes narrower in time ($\sim 100 \mu\text{secs}$).

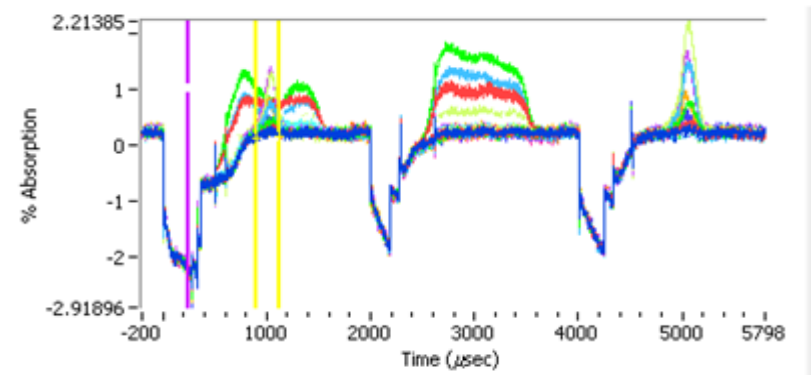


Figure 10. Shows the raw sequence of gas pulses, in this case, pinhole and slit nozzles fired together followed by the pinhole only and then slit only. Each color is taken at different fixed mm-wave frequency around the $N=4 \leftarrow 3$ rotational transition of N_2O . The negative going signals are trigger pulses intentionally subtracted from the positive going absorption signals. The length of each trigger pulse allows us to determine which nozzle has fired.

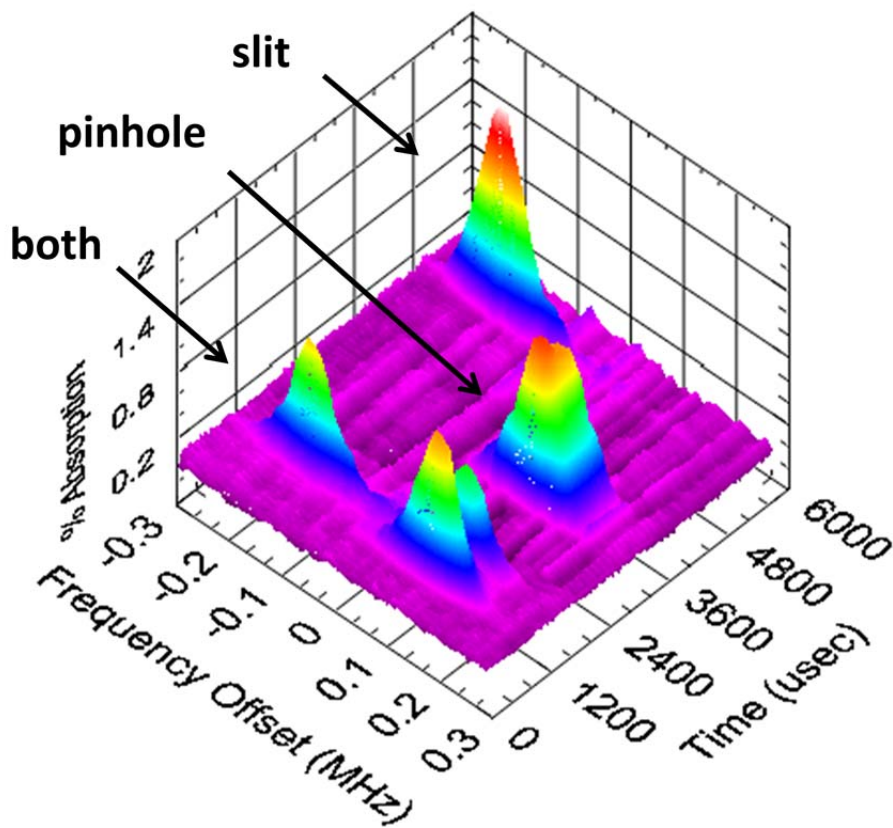


Figure 11. Shows a surface plot of the same signals in Figure 10 but with the negative going timing pulses removed. Signals are from a single rotational line ($N=4 \leftarrow 3$) of N_2O . The data has been sequentially collected by alternately firing both nozzles together, then firing the pinhole nozzle, followed by the slit nozzle. The signals have been averaged and background subtracted. Doppler shifts in frequency are due to the opposite angular orientation of the two molecular beams relative to the mm-waves.

During data analysis, we cleaned up the noise by subtracting the background (Figure 11). By subtracting the background, we obtained a more accurate representation of the signal and remove trigger induced dips from the data. In addition to removing background, we were able to focus on a single or multiple peaks (Figures 11). Product and parent peaks can be masked or distorted by other signals and/or noise. By removing background and

signals, we hoped to isolate and focus on our target signal that may have been distorted or masked. Figure 12 show the various signal isolations possible during data analysis.

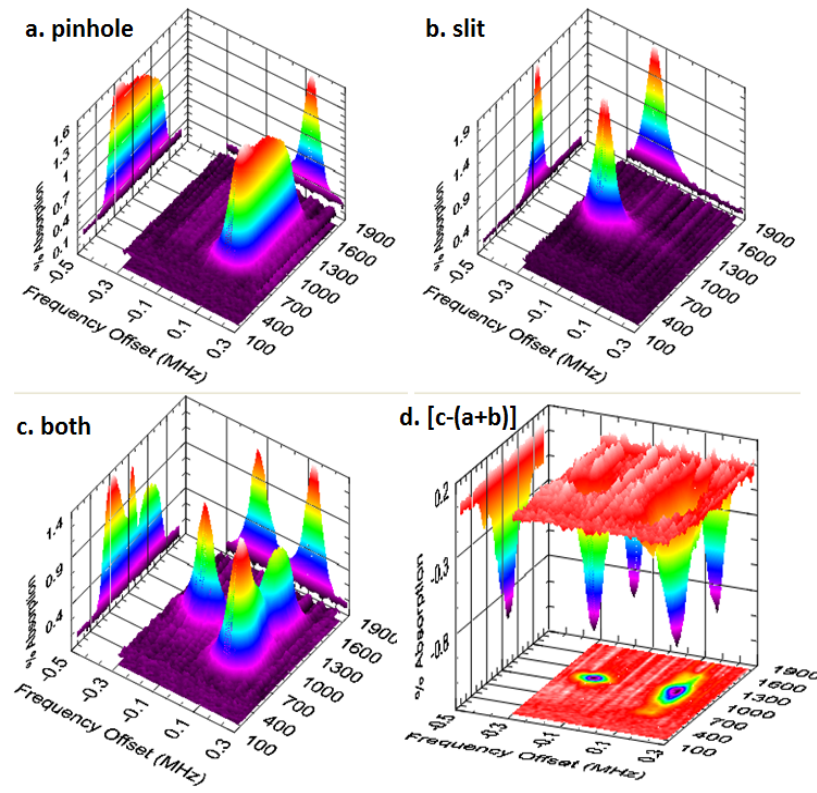


Figure 12. Shows an example of the potential avenue of data analysis. Plots. (a) through (c) show the isolation of specific signals, so we can either look at the collision free signals, or the scattered signal. Plot (d) shows the both signal minus the pinhole and slit signal, by subtracting those peaks we can isolate any scattered product signal that may be masked, which if present, would appear as positive signal in plot (d).

II.B.2 Experimental Data for the I + O₃ Reaction

Due to issues with the pinhole nozzle, we were unable to take very many scans of the I + O₃ reaction. Figure 13 shows scans for the IO product. Initially we thought that the product signal may have been obscured by noise. So during data analysis we zoomed in, in time, to where the product should have emerged. Unfortunately, the features in figure 13 were not reproducible; if signal is present, it is smaller than the fluctuations in the baseline due to nozzle vibration (left figure) and/or noise spikes due to RF pickup (right figure). It is also possible, as will be mentioned in section III.B.3 with NO, the product IO may have come out too hot vibrationally and/or rotationally. In the former case, for $v > 1$, rotational transition frequencies are not available in the literature, while in the latter case, we do not have mm-wave sources extending to frequencies above 330 GHz or $N' \leftarrow N'' > 15 \leftarrow 14$. It is also possible the products came out in an excited spin-orbit state of IO which we did not attempt to probe.

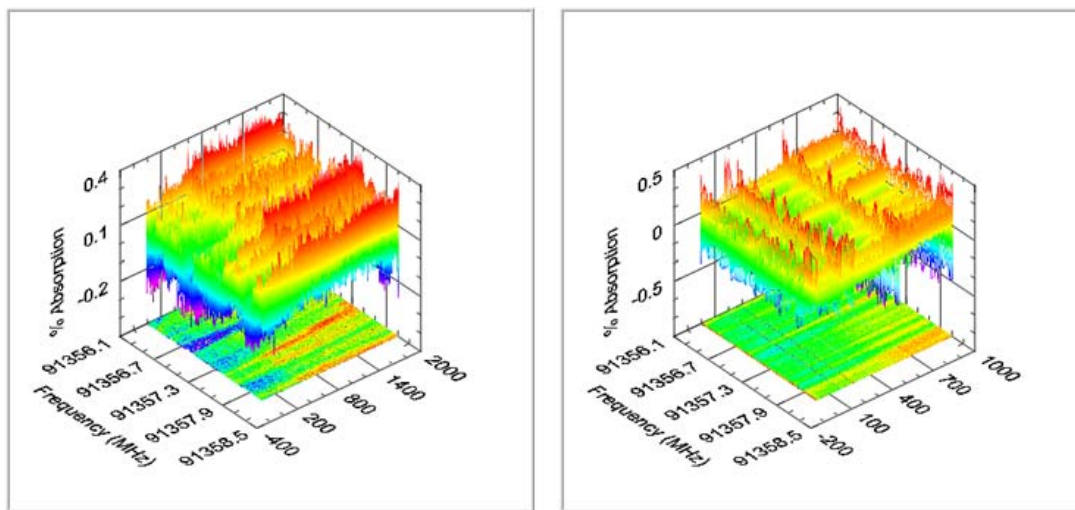


Figure 13. Scans to find the IO product signal using CMB methods. $N=4 \leftarrow 3$, $J=4.5 \leftarrow 3.5$, $K=-1 \leftarrow 1$, $1 \leftarrow -1$, $F_1=7 \leftarrow 6$.

II.B.3. Experimental Data for the Br + O₃ Reaction

Since we were unsuccessful in detecting signal in the I + O₃ experiment, we decided to move onto the Br + O₃ experiment. A vial of bromine was attached to the gas inlet system and neat Ar passed through the sample to facilitate evaporation and act as a carrier gas for the bromine vapor (Figure 14).

As mentioned in section II.C. we used real-time RGA scans to confirm the presence of atomic bromine and product (BrO). The real time mass scan proved inconclusive to the formation of BrO as did the absorption signal on the oscilloscope, even after accounting for Doppler shift and the possibility of the molecule coming out in excited or ground vibrational states. Because of this we decided to take a new direction and attempt to form the XO product with excited state oxygen atoms (O(¹D)).

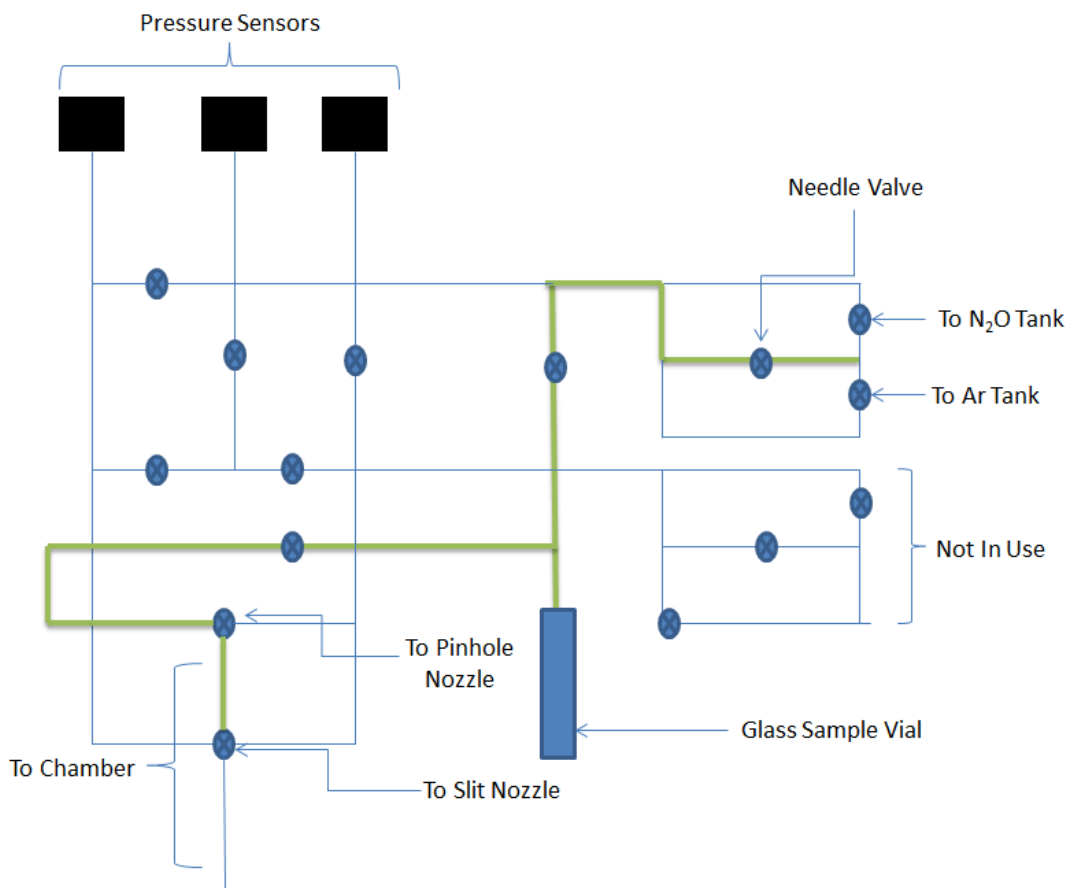
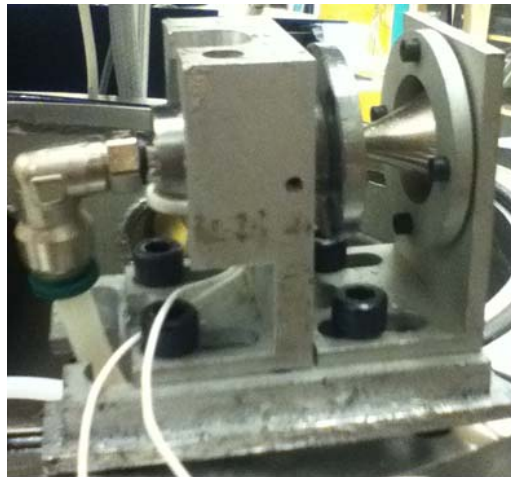


Figure 14. Schematic of the gas inlet manifold, the green lines represent the pathway of the argon and bromine as it goes into the pinhole nozzle for CMB experiments.

II.C. Problems with X + O₃ Experimental Modifications

The previous modification to the pinhole nozzle was ineffective. The iodine reservoir, over time failed to maintain a vacuum tight seal, and when fired it would overwhelm the pinhole molecular beam and the vacuum system. In addition to troubles maintaining vacuum, the heater melted the plastic connector of the iodine reservoir, further ruining the vacuum seal (shown in Figure 8). We also experienced the nozzle clogging, as a result of iodine vapor plating out. To maintain chamber pressure, we replaced the iodine reservoir with a 90° quarter inch push-in banjo-type connector (Figure 15). From this change, we had managed to get a better pinhole molecular beam signal (Figure 16).



a. Side



b. Back

Figure 15. 90° Push in connector and banjo fitting, the replacement of the iodine reservoir, lead to better signal from the pinhole nozzle

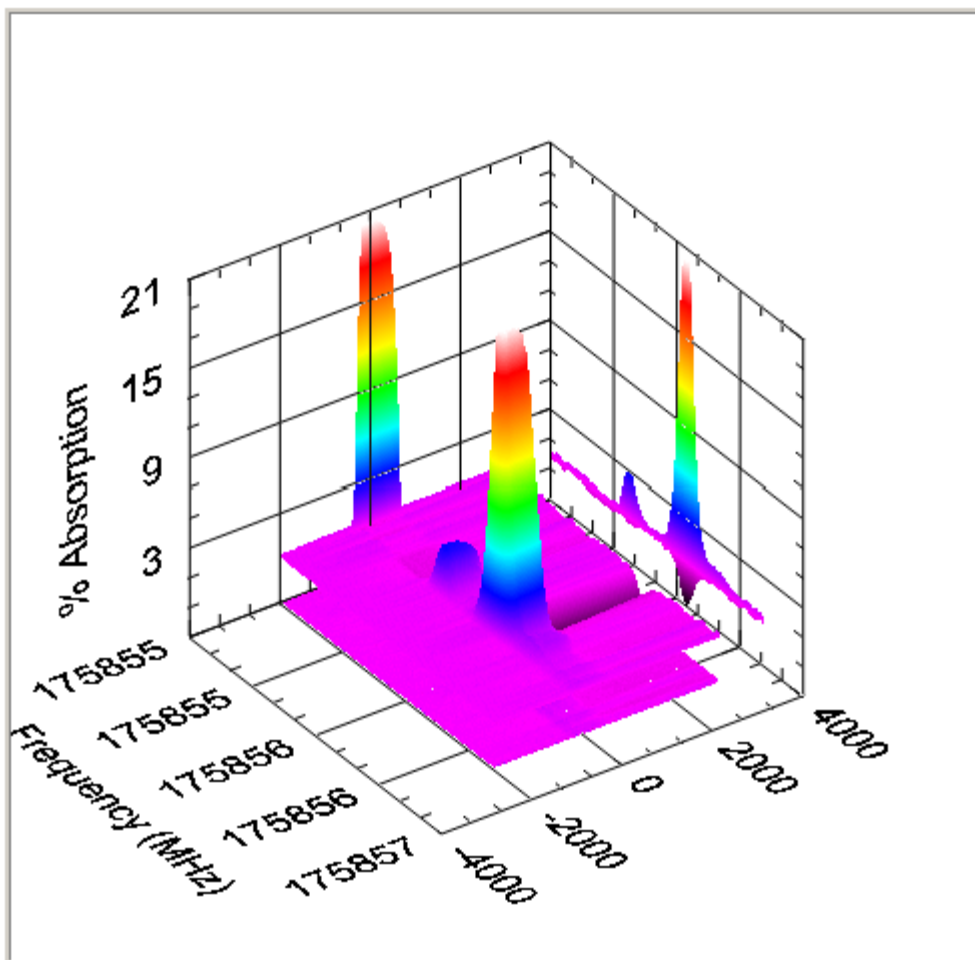


Figure 16. Signal from the pinhole using N_2O after replacing the iodine reservoir with 90° push in connector, secondary peak a result of N_2O leaking into the slit arm and out of the nozzle, due to Doppler Shift corresponding to slit nozzle location. $N=7 \leftarrow 6$

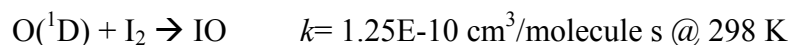
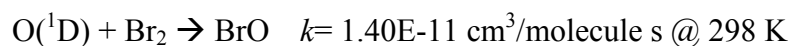
The previous experimental setup required the atomic halogens (I and Br) to be produced outside the nozzle exit within the chamber. We used the Spectra International Residual Gas Analyzer Mass Spectrometer (RGA) to confirm the presence of bromine atoms (m/z : 79/ 81 amu). After several real-time scans, we could see a noticeable uptick in intensity of the mass units associated with the isotopes of atomic bromine when the

laser was on, and a rapid decrease in the mass units when the laser was off.

Unfortunately, the RGA was not in sync with the pinhole nozzle firing, so the atomic bromine signals were not stable. Because of this we were unable to know if we were in fact producing atomic bromine exclusively. Nevertheless, we concluded that, at the very least, we were indeed making some atomic bromine. After confirming an ozone signal, we ran both nozzles, and attempted to detect the BrO signal by means of both the RGA and millimeter-wave absorption.

After several unsuccessful attempts to detect signal, we speculated that the laser (Melles Griot 43 ion series) was not intense enough to produce the density of halogen atoms necessary to effectively make enough XO (X= I and Br) products for detection. In an effort to find a more robust reaction the X + O₃, we performed a literature review, and found that the kinetics for the O(¹D) + X₂ (X= I₂ and Br₂) reactions are significantly more effective than X + O₃ (X= I and Br) reactions, largely because O(¹D) is almost barrierless when reacting and, therefore, much more likely to form the desired XO product:

[31,32]



The rate constants for $O(^1D) + X$ ($X = \text{Br}$ and I) showed that these reactions were expected to proceed at the gas-kinetic collision rate coefficient, which for hard-spheres of diameter 0.4 nm, is $2.5E-10 \text{ cm}^3/\text{molecule s}$. [33]

Another problem with the previous setup was the use of the chopper blade. The chopper blade was designed to cut off part of the molecular beam for the experiment, with the rest of the gas being pumped away; however, it appeared that the backscattered gas would move around the chopper disk obscuring the slit molecular beam and overwhelming the vacuum system. Initially, to fix the problem, we shortened the gas pulse, but that led to a loss of signal intensity and the signal was affected by more artifact noise. Subsequently, after deciding to use $O(^1D)$ instead of ozone, the chopper blade was removed.

The primary purpose of the chopper blade was to improve the signal relative to the noise. This was in response to slow baseline noise variation on the time scale of a full gas pulse. Because the Ar/Kr ion laser was continuous wave (CW), we produce bromine or iodine atoms and hence products throughout the full gas pulse, making it challenging to see small differences in the product signal relative to the slowly varying baseline noise. By contrast, during the $O(^1D)$ experiments, the laser was on only for short periods of time (~3-5 nsecs) making the potential product signal stand out against a slowly varying background. These factors made the chopper obsolete in the $O(^1D)$ experiments.

The final problem we had with the initial experimental setup was the slit skimmer. The previous slit skimmer did not have the desired effect of cleaning up the slit signal. To prevent undesirable artifacts from interfering with the slit signal, we made a custom slit

skimmer with aluminum. The new slit skimmer decreased the frequency broadening of the slit signal (Figure 17).

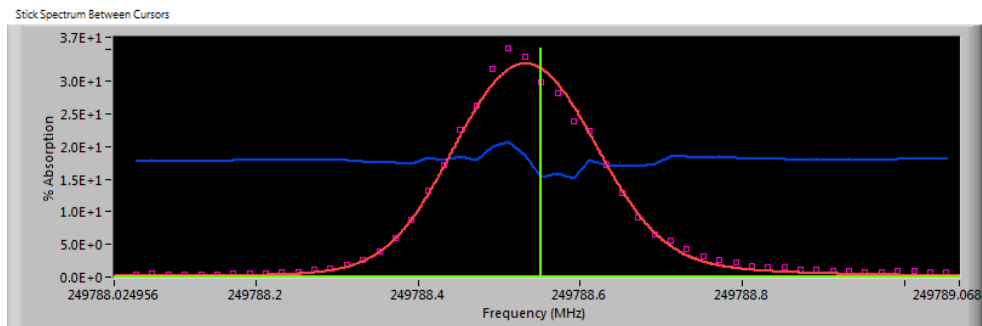


Figure 17. Voigt profile characterized by $T_{\text{trans}} = 47$ K spread, 15 kHz Lorentzian broadening (gas: ozone). Dotted line is experimental signal. Blue line is the residual offset. Red curve is the Voigt fit of slit nozzle signal to the JPL frequency line ($N=7 \leftarrow 6$, $K_{-1}=1 \leftarrow 0$, $K_{+1}=7 \leftarrow 6$).

II.D. Conclusions for the $X + O_3$ Reactions

While the $X + O_3$ reaction was unsuccessful for our particular experimental setup, we learned valuable information for future reference. In our attempt to photodissociate halogen molecules (I_2 and Br_2), we learned that the CW laser we were using may not have been intense enough to produce the density of halogens atoms necessary to form enough XO products for detection.

We also found that the $X + O_3$ reaction is not the best type of experiment to try using our CMB detection method (absorption spectroscopy). When comparing the rate constants of the $X + O_3$ reaction to the gas kinetic rate (where every collision is a reaction) we found that with both iodine and bromine only one in every one hundred collisions will result in product formation. This combined with the uncertainty in the

density of halogens atoms produced by the CW laser, may have contributed to little or no product formation to be detected.

Finally as mentioned in section III.B.3., running reaction as a crossed molecular beam (CMB) results in products coming out in higher spin-orbit vibrational, and/or rotational states. At this time there were no literature values on the rotational lines of BrO and IO higher than the $v=1$ state, we were unable to check higher states. In lieu of obtaining a higher power CW laser and/or extending our millimeter-wave frequency coverage, a solution to this issue may be to run the $X + O_3$ reaction under single molecular beam (SMB) conditions, as the collision within the beam would slow down the radical halogen increasing its collisional cross section and hopefully result in more product formation.

CHAPTER III

O(¹D) + X REACTION

III.A. O(¹D) + X Experimental Setup

To optimize the system for the formation of O(¹D), and ultimately the XO products, we oriented the slit nozzle 90° with respect to the microwaves. This had the benefit of aligning the slit opening with the laser, as well as not having to account for Doppler Shifting in the product or parent molecule (Figure 18).

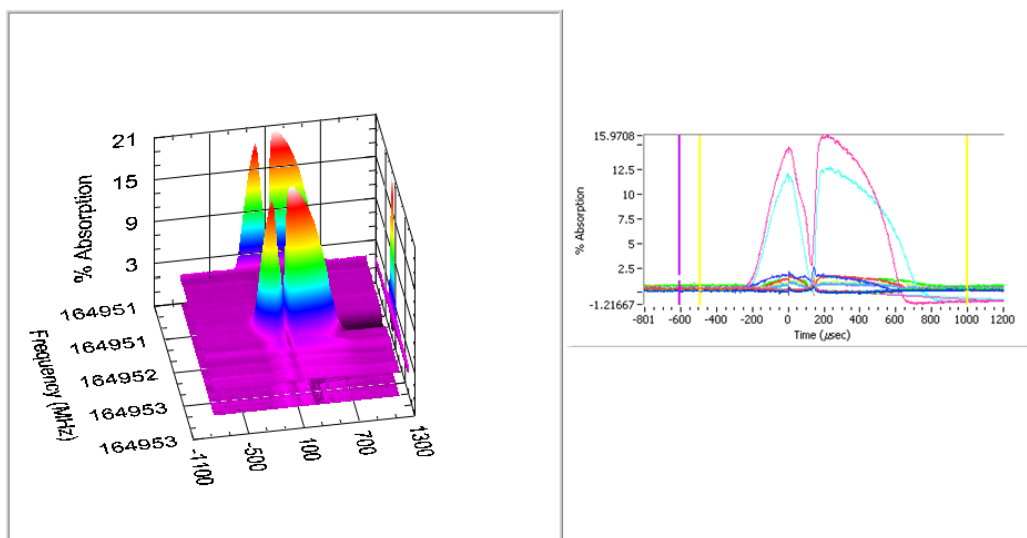


Figure 18. Ozone mm-wave transient absorption signal ($v=0$ transition). The gap or “hole” at 100 μ sec corresponds to the depletion of ozone following the laser firing. It is during this window of time we expect production of O(¹D) radical and subsequent product formation. $N=7 \leftarrow 6$, $K_{-1}=1 \leftarrow 0$, $K_{+1}=7 \leftarrow 6$

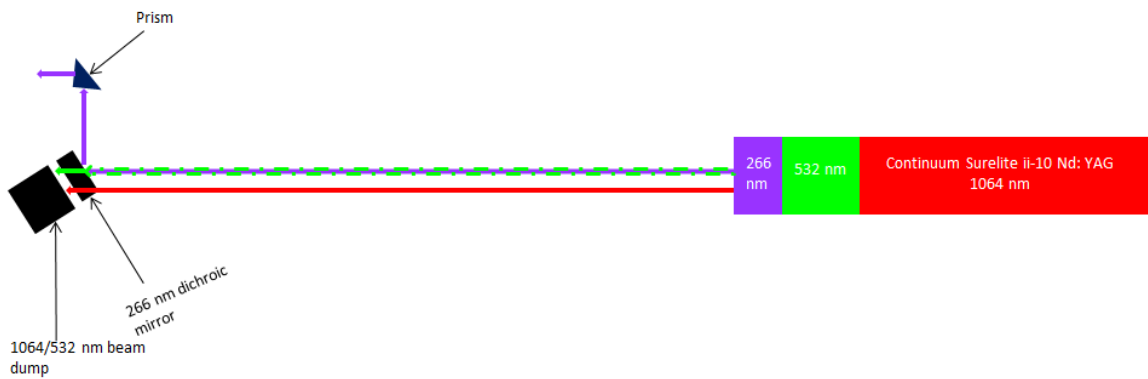


Figure 19. Schematic of the laser pathway before entering the chamber

Figure 19 shows the pathway of the 266 nm UV light before it enters the chamber. Nd: YAG laser generates 1064 nm Infra-Red (IR) light, which is doubled into 532 nm green light, before being quadrupled into the usable 266 nm UV. From there, the green and IR light passes through a 266 nm dichroic mirror and are dumped. The UV light is reflected 90° to a prism, which then directs the beam into the chamber.

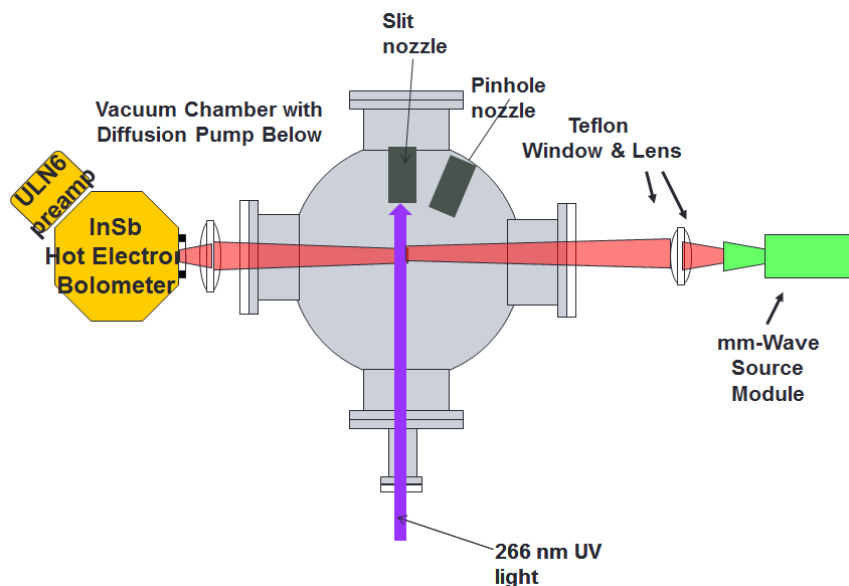


Figure 20. Top down view of the $O(^1D) + X$ experimental setup

Figure 20 shows the top down view of the experiment. The figure details the projection of the microwave and laser beams into the chamber. The slit nozzle was placed 90° with respect to the microwaves (light red) and 180° to the UV light.

Ozone was generated using the same methods as described in the $X + O_3$ experiment and fired through the slit nozzle. Before each daily experimental run, we would take an ozone diagnostic scan, with the laser going into the chamber (Figure 21). By doing so, we could monitor the experimental conditions from day to day and identify and fix any anomalies as well as optimize the hole. Figure 22 shows one such anomaly, where the plastic skimmer sustained too much damage to properly skim the molecular beam.

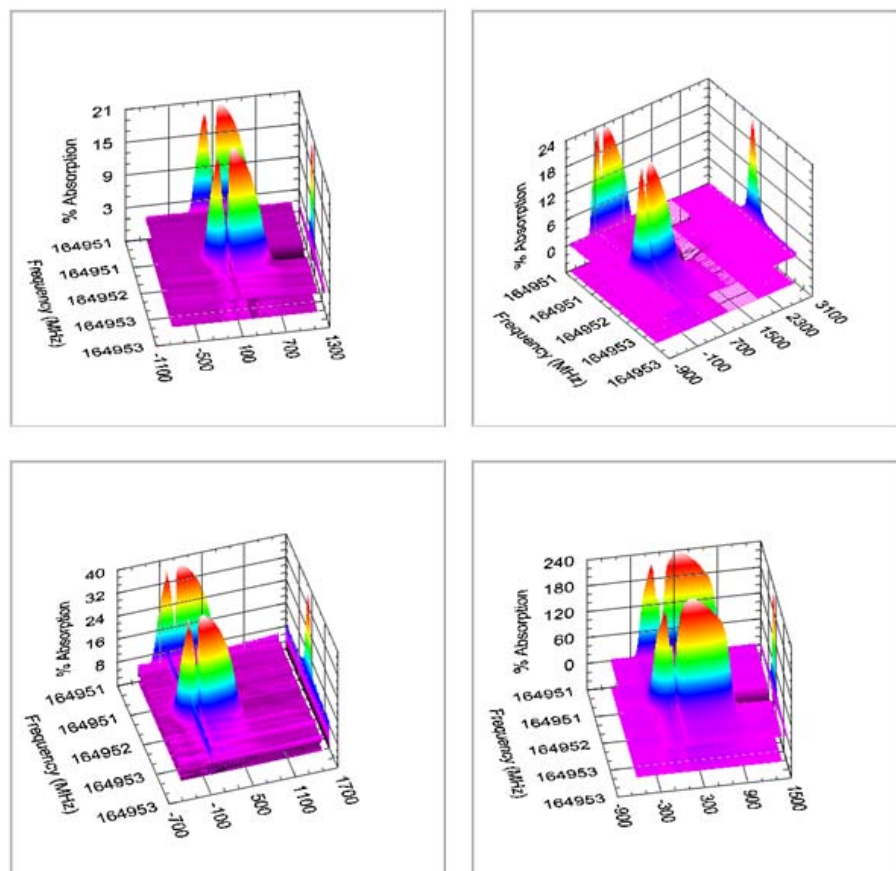


Figure 21. Examples of daily diagnostic scans. Ozone signal intensities can vary significantly with time as the gas inlet Teflon tubing first passivates with ozone and later as the ozone runs out. The depth of the hole also lets us know how well the laser is tuned and aligned. Top Left: $N=7 \leftarrow 6$, $K_{-1}=1 \leftarrow 0$, $K_{+1}=7 \leftarrow 6$ Top Right and Bottom: $N=3 \leftarrow 2$, $K_{-1}=1 \leftarrow 0$, $K_{+1}=3 \leftarrow 2$

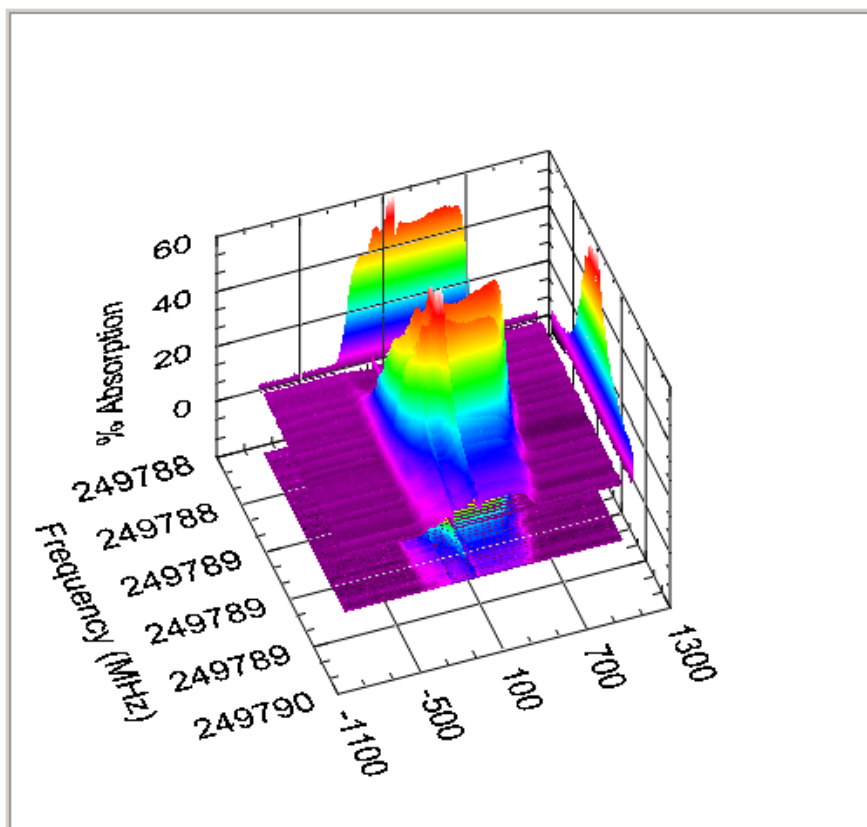


Figure 22. Diagnostic scan that indicates a problem with the experiment. $N=7 \leftarrow 6$, $K_{i=1} \leftarrow 0$, $K_{+1}=7 \leftarrow 6$

For the single molecular beam experiments, the gases were mixed and introduced to the slit nozzle via the gas inlet system, with the exception of iodine. Bromine and Chloroform were introduced to the slit nozzle from the gas inlet system. A vial of reagent was attached to a specially rigged system, where argon was passed through the liquid to facilitate evaporation and act as a carrier to the gas inlet system (Figure 23). From there the slit nozzle was opened to the gas inlet system, and the reagent was introduced to the chamber. Ozone bypassed the gas inlet system by connecting directly to the slit nozzle.

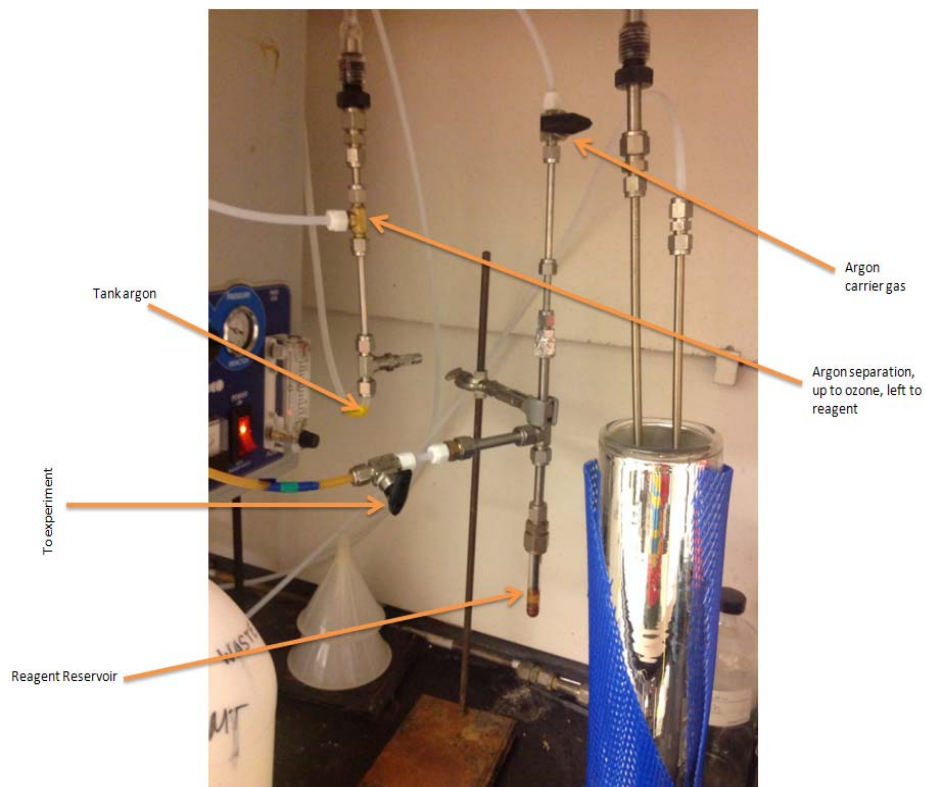


Figure 23. New set up to introduce non-gaseous reagent into the experimental chamber (located in laboratory chemical hood).

For the iodine single molecular beam (SMB) experiments, the same apparatus used for both bromine and chloroform was moved from the hood and attached directly to the slit nozzle, bypassing the gas inlet system. The vial was then heated to increase iodine's vapor pressure, and ozone and argon were passed through the iodine crystals acting as carrier gases. We did this in the hopes of preventing iodine vapor from plating out; this method proved unsuccessful, even with the addition of heating tape to the iodine reservoir.

III.A.1. Laser Optimization for the Production of O(¹D)

After deciding to run O(¹D) + X (X= I₂ and Br₂) reactions, we needed to modify the experiment to optimize the production of O(¹D). Initially, we planned on using the Continuum Panther EX OPO (optical parametric oscillator) laser to produce tunable UV light delivered through an optical fiber to the exit of the nozzle. This method could take advantage of ozone's photodissociation over the entire Hartley Band. We set the millimeter-waves to a strong rotational line of ozone, and the OPO was set to scan 1 nm increments of the Hartley Band. The UV was scanned and timed to fire at the peak of the slit nozzle gas pulse. Still, we found that the delivered intensity was not strong enough to produce a visible depletion of the ozone signal, and hence not of adequate strength to produce sufficient quantities of O(¹D) atoms such that the produced XO molecules could be detected (Figure 24).

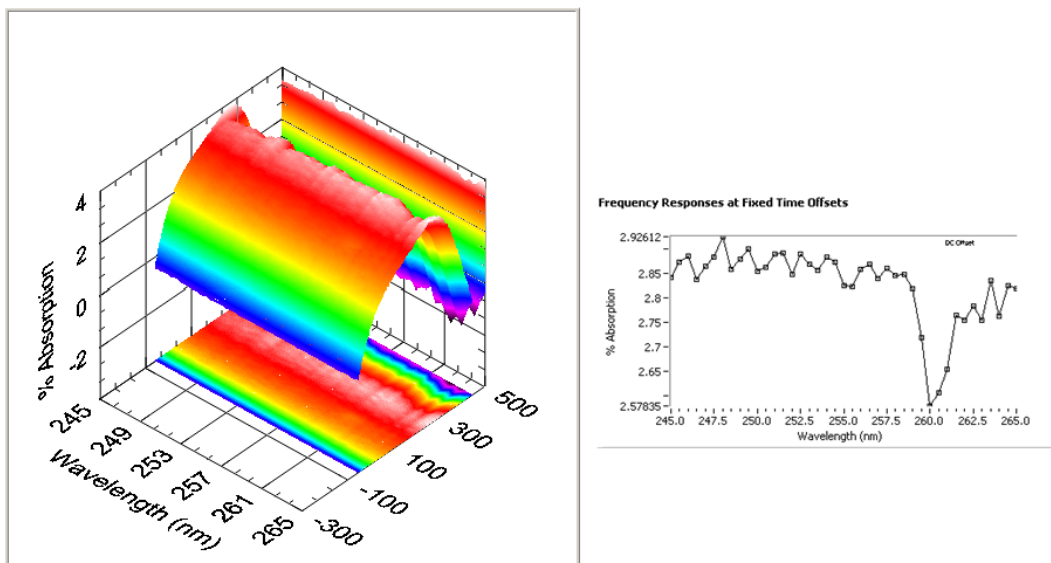


Figure 24. Photodissociation OPO laser scan (over part of Hartley band) of ozone at a fixed mm-wave frequency centered on an intense ozone rotational transition (249788.5520 MHz). The left figure shows the mm-wave transient absorption at each UV wavelength. The laser was set to fire at the peak of the gas pulse and after some baseline subtraction, the figure on the right depicts the ozone peak intensity as a function of UV wavelength. While depletion should occur at all UV wavelengths covered, the hole only occurs at 260 nm, which simply corresponds to the power optimization of the harmonic crystals in the OPO laser and not the actual UV spectrum of ozone.

As can be seen from Figure 24, we scanned areas where peak ozone absorption occurs in the Hartley band, and the only hole produced was at 260 nm. This corresponds to the power optimization of the two harmonic crystals, so that the maximum UV power output of the frequency doubled OPO laser (2.4 mJ/pulse) was hitting the molecular beam, producing the largest hole. To dramatically increase the laser power and hence hole depth, we decided to forego the tunable OPO laser and take advantage of the far greater power (~80 mJ/pulse) available at 266 nm from the tripled frequency output of the Continuum Surelite II-10 Nd:YAG laser. Figure 18 shows the hole we were able to

produce. The hole bisects the ozone peak, demonstrating full depletion of the ozone signal following firing of the laser. Because the laser was collinear with the molecular beam, ozone over the full length of the molecular beam was depleted. This resulted in an effect on the mm-wave signal that lasts for over 100 μ secs despite the fact the laser output is only on 3-5 nsecs. Satisfied that we were dissociating O_3 we began running the $O(^1D) + X$ experiments.

We ran the bromine, iodine, chloroform, and nitrous oxide experiments using the single molecular beam and crossed molecular beam methods. By using an SMB experiment, we hoped that we would increase the probability of collisional interactions, and therefore, product formation. With respect to the nitrous oxide, Tokel and researchers found that when running CMB experiments, the product NO, was more likely to come out vibrationally hot as compared to an SMB experiment. [34] We also suspected that this might be the case for the IO, BrO, and ClO products. Unfortunately as discussed earlier, there is no rotational data higher than $v=1$ for either IO or BrO in the Jet-Propulsion Laboratory spectral database (JPL), so we have been unable to check rotational lines at higher vibrational states.

III.B Experimental Data for the $O(^1D) + X$ ($X = Br_2, I_2, N_2O,$ and $CHCl_3$) Reactions

III.B.1. Experimental Data for the $O(^1D) + Br_2$ Reaction

As mentioned earlier in section II.C., the rate constant for the $O(^1D) + Br_2$ is an order of magnitude better than the $Br + O_3$ reaction. So we felt that we would be able to detect signal if the product molecule (BrO) was present. Before doing so, we optimized the CMB experiment, for the hole and the pinhole molecular beam (Figure 25). The wide sloping dip shown in Figure 25 is what we thought was the pinhole signal overlapping the hole and the ozone molecular beam (slit nozzle). We suspect however, that some of the dip was a result of exhaust gas from the pinhole nozzle moving through the arm to the slit and suppressing the ozone molecular beam.

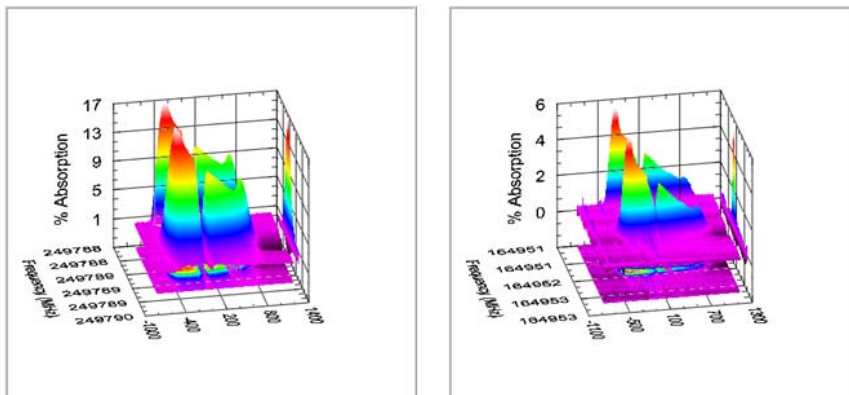


Figure 25. Pseudo-optimization of the pinhole, slit, and laser for CMB experiments. Right figure shows optimization at a tripled ozone frequency. While the left figure shows optimization at a doubled ozone frequency. The difference in % Absorption is a result of a decrease in ozone from the laboratory hood. Left: $N=7 \leftarrow 6, K_{-1}=1 \leftarrow 0, K_{+1}=7 \leftarrow 6$, Right: $N=3 \leftarrow 2, K_{-1}=1 \leftarrow 0, K_{+1}=3 \leftarrow 2$

We ran several experiments looking for the $v=0$ to the $v=1$ rotational states of BrO with no success (Figure 26). Since higher vibrational states are expected to be populated the JPL database does not have any rotational lines of BrO higher than $v=1$, we decided to try and find $v=2$ ourselves. The frequency shift from $v=0$ to $v=1$ for the $N=6 \leftarrow 5$ transition was -1.408 GHz. We assumed a similar -1.408 GHz shift for the $v=1$ to $v=2$ transition and then scanned within 10 MHz from this assumed shift see Figure 27. Finally, in the hopes of increasing rotational relaxation and/or slowing the $O(^1D)$ atom by collisions (slower $O(^1D)$ atoms are expected to have a larger collision/reaction cross section) between the gases, we switched to an SMB experiment via the slit nozzle (Figure 28). We still did not find anything, so we moved on to the $O(^1D) + I_2$ experiment, as it had a gas kinetic rate constant ($k= 1.25E-10 \text{ cm}^3/\text{molecule s}$).

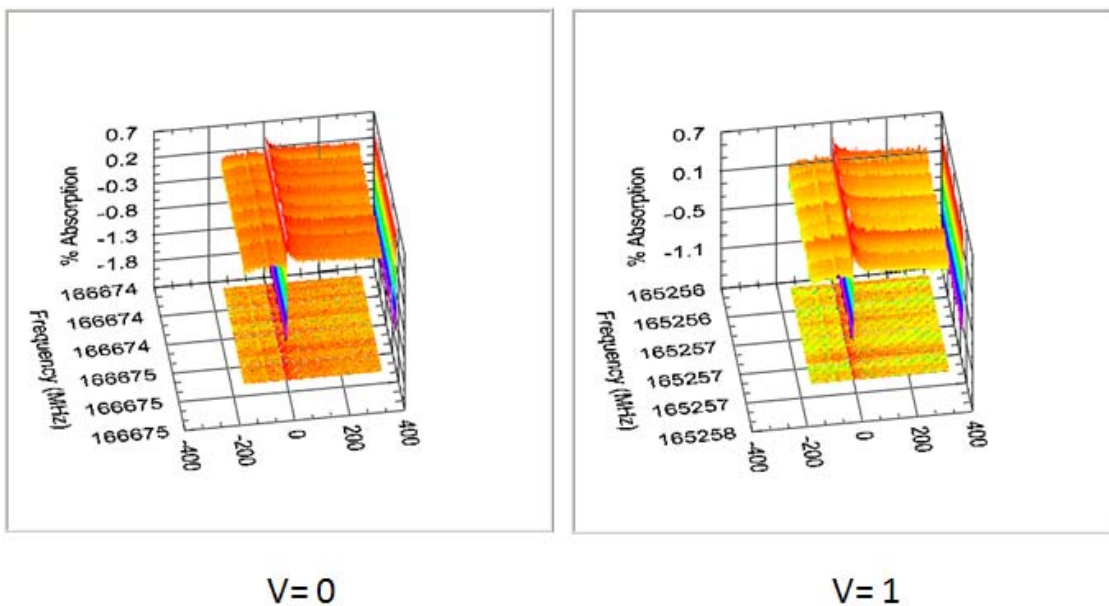


Figure 26. Sweeps for the ^{79}BrO signal at the $v=0$ and $v=1$ states. For $v=0$: $N=6 \leftarrow 5$, $K=-1 \leftarrow 0$, $J=6.5 \leftarrow 5.5$, $F_1=8 \leftarrow 7$ Center frequency ($v=0$): 166674.17990 MHz, For $v=1$: $N=6 \leftarrow 5$, $K=-1 \leftarrow 1$, $J=6.5 \leftarrow 5.5$, $F_1=8 \leftarrow 7$ Center frequency ($v=1$): 165256.56460 MHz, Span frequency (both): 1 MHz, Averaged # of Sweeps (both): 60, # of Steps (both): 50, Scan increments (both): 0.02 MHz. The early time spikes are always present whether the gas is present or not. They are laser generated millimeter wave signals from dumping the 532 nm and 1064 nm laser beams into a Teflon beam dump.

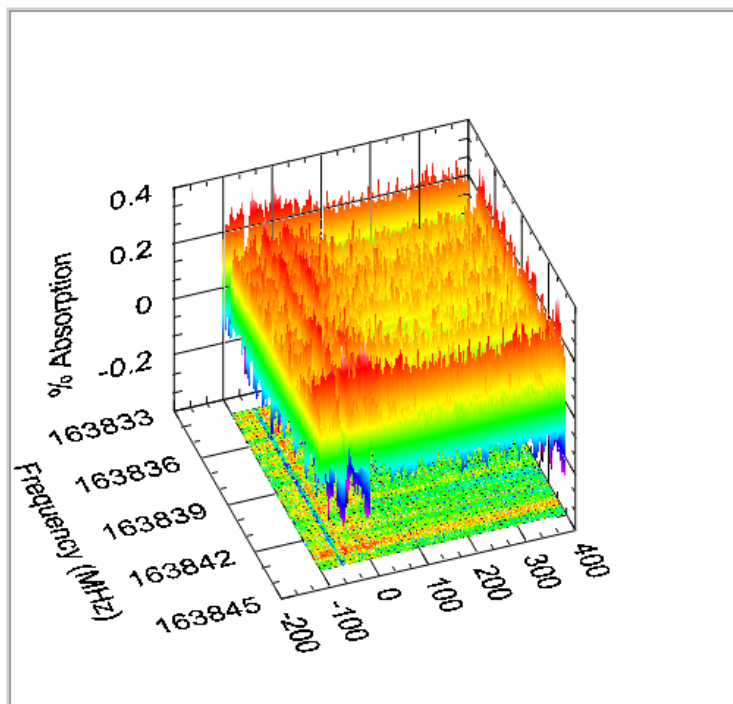


Figure 27. Broadband frequency sweep of BrO for the $v=2$ state using CMB method. Center frequency: 163838.94930 MHz @ $v=1$, Span frequency: 10 MHz, Averaged # of Sweeps: 60, # of Steps: 50, Scan Increments: 0.20 MHz. $N=6 \leftarrow 5$, $K=-1 \leftarrow 1$, $J=6.5 \leftarrow 5.5$, $F_1=8 \leftarrow 7$

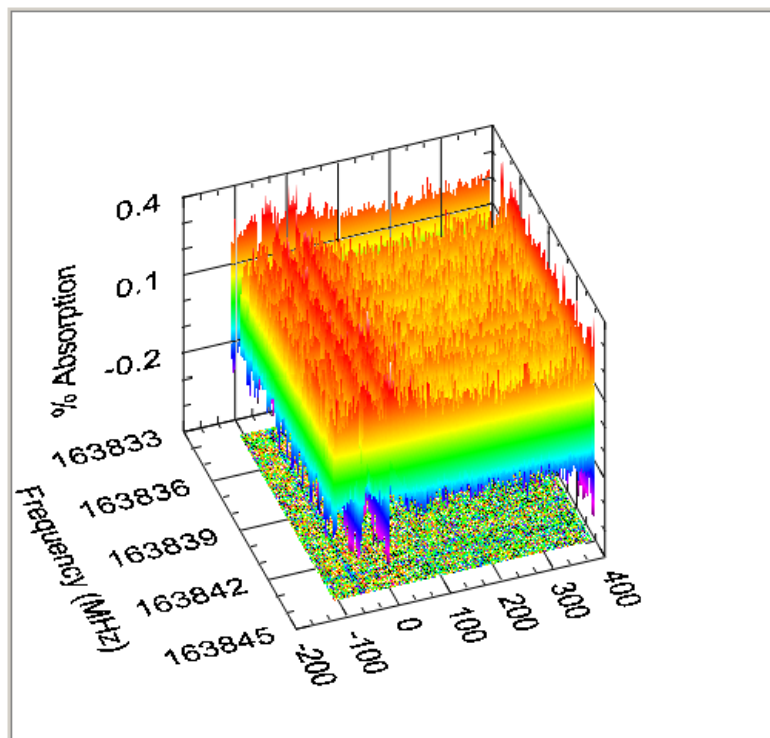


Figure 28. Broadband frequency sweep of BrO for the $v=2$ state using SMB method. Center frequency: 163838.94930 MHz @ $v=1$, Span Frequency: 10 MHz, Averaged # of Sweeps: 60, # of Steps: 200, Scan increments: 0.050 MHz. $N=6 \leftarrow 5$, $K=-1 \leftarrow 1$, $J=6.5 \leftarrow 5.5$, $F_1=8 \leftarrow 7$

III.B.2. Experimental Data for the $O(^1D) + I_2$ Reaction

As mentioned earlier, we switched to iodine because it has a gas kinetic rate constant, essentially every collision should result in a reaction. Because of iodine's tendency to plate out at room temperature, we decided to move the reagent holder closer to the chamber. In addition to moving iodine closer to the chamber, we decided to use an O_3/Ar mix as our carrier gas, in the hopes that increasing collisional interactions sooner would result in quicker product formation, than with other SMB experiments. We also ran the experiment using the CMB method, with Ar as our carrier gas. Despite our best

efforts to prevent the plating of iodine, it still occurred most likely as the primary cause of why we did not obtain signal (Figure 29).

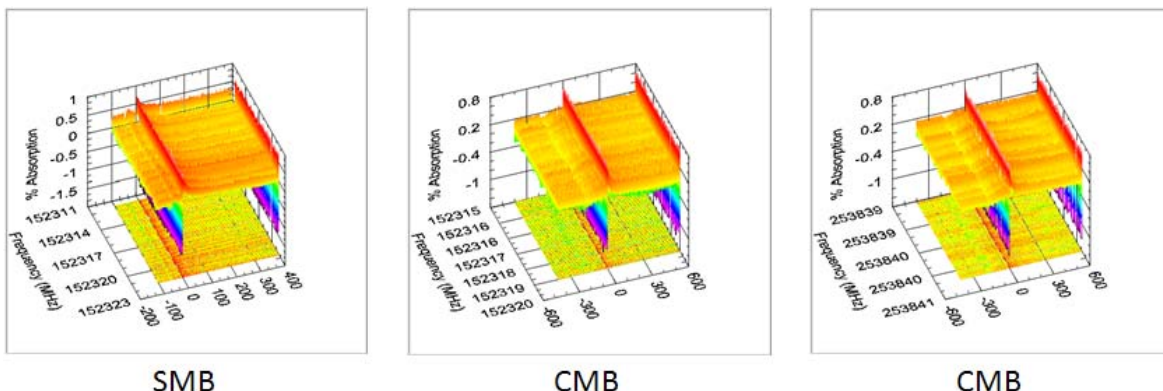


Figure 29. Different scans to find IO signal using both CMB and SMB experimental methods. For SMB: Center frequency: 152316.64130 MHz Span frequency: 10 MHz Averaged # of Sweeps: 60 # of Steps: 100 Scan increments: 0.10 MHz. For CMB (center): Center frequency: 152316.72540 MHz Span frequency: 4 MHz Averaged # of Sweeps: 60 # of Steps: 100 Scan increments: 0.04 MHz. For SMB/CMB (center): $N=7 \leftarrow 6$, $K=-1 \leftarrow 1$, $J=7.5 \leftarrow 6.5$, $F_1=10 \leftarrow 9$ For CMB (left): $N=12 \leftarrow 11$, $K=1 \leftarrow -1$, $J=12.5 \leftarrow 11.5$, $F_1=15 \leftarrow 14$ Center frequency: 253839.53620 MHz Span frequency: 2 MHz, Averaged # of Sweeps: 60 # of Steps: 50 Scan increments: 0.04 MHz.

III.B.3. Experimental Data for the $O(^1D) + N_2O$ Reaction

Thinking that the vaporization of solids (iodine) and liquids was affecting our ability to see signal, we decided to try a gas reagent for our SMB and CMB experiment. For this purpose we used nitrous oxide, as it was readily available and is quickly becoming the dominant cause of ozone destruction, since the gradual phase out of CFCs.⁶

We used both SMB and CMB methods with no success (Figure 30). A literature search showed that not only was the product molecules' (NO) most intense lines outside our frequency range, it also showed that the type of experiment effects the product energy

distribution. [34,35] In single molecular beam experiments the product (NO) was more likely to come out in the ground state ($v=0$), and in crossed molecular beam experiments the product was more likely to come out in an excited state ($v=7$). [34] From this we speculated that BrO and IO may have a similar effect. To test this theory, we decided to run an $O(^1D) + CHCl_3$ experiment in the hopes that the ClO product forms.

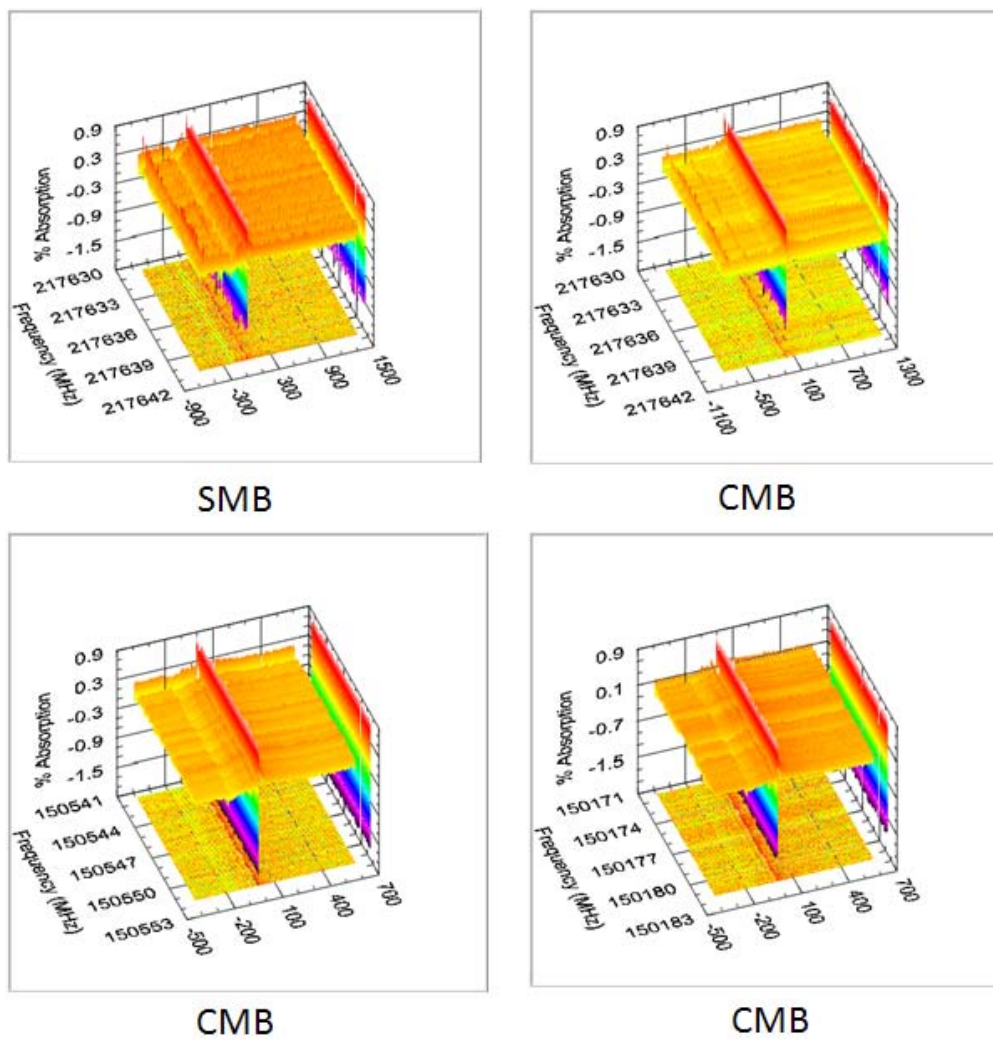


Figure 30. Different scans to find NO product using SMB and CMB experimental methods (all scans are $v=0$ state). For SMB/CMB (top): Center frequency: 217635.56940 MHz For CMB (bottom left): Center frequency: 150546.520 MHz. For CMB (bottom right): Center frequency: 150176.480 MHz. For All: Span frequency: 10 MHz Averaged # of Sweeps: 60 # of Steps: 100, Scan increments: 0.10 MHz. $J=1.5 \leftarrow 0.5$, $F_1=3 \leftarrow 2$, $L=1 \leftarrow -1$

III.B.4. Experimental Data for the $O(^1D) + CHCl_3$ Reaction

In the past the Duffy Lab has conducted experiments, which provided rotational data up to the $v=7$ excited state of ClO. From this data, we felt confident that we could detect vibrationally excited ClO if it were present. Rather than work with molecular chlorine in the reaction $O(^1D) + Cl_2$, for corrosion and safety reasons we chose instead to look for other chlorine source that could react with $O(^1D)$. We chose chloroform ($CHCl_3$), as we already had a set up capable of vaporizing liquid.

We ran both the SMB and CMB experiments using the same methods described for the $O(^1D) + Br_2$ reaction. So far we have managed to scan up to the $v=4$ state using both the CMB and SMB methods (Figure 31), before issues with the ozone generator caused us to shut down. We even tested the excited $\Omega= \frac{1}{2}$ electronic state, which the product may have come out in (Figure 31).

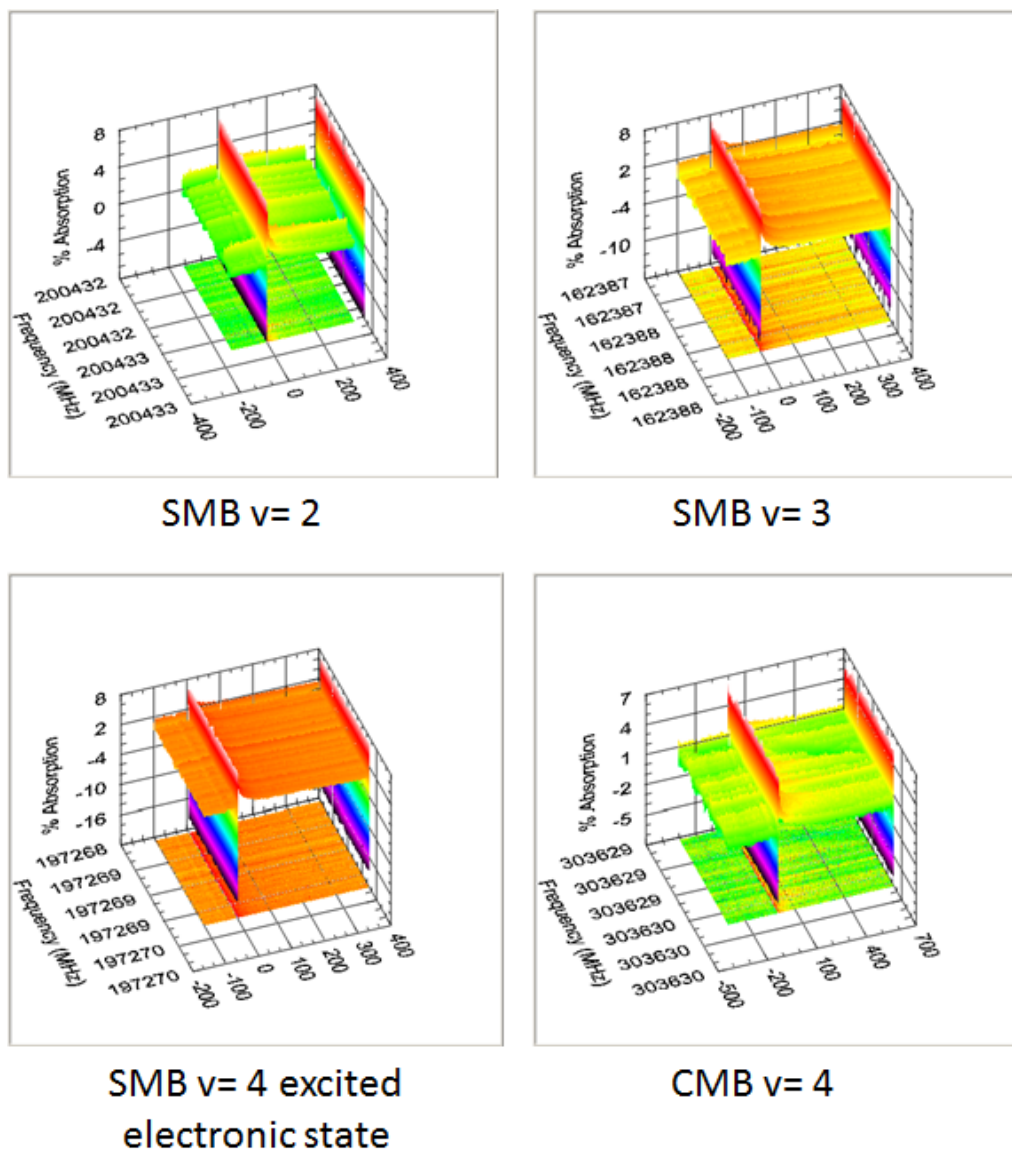


Figure 31. Different scans to find ClO product using SMB and CMB experimental methods. For SMB v=2 (top left): $N=5 \leftarrow 4$, $K=1 \leftarrow -1$, $J=5.5 \leftarrow 4.5$, $F_1=7 \leftarrow 6$ Center frequency: 200432.33270 MHz. For SMB v=3 (top right): $N=4 \leftarrow 3$, $K=-1 \leftarrow 1$, $J=4.5 \leftarrow 3.5$, $F_1=6 \leftarrow 5$ Center frequency: 162387.45240 MHz. For SMB v=4* (bottom left): $N=6 \leftarrow 5$, $K=1 \leftarrow -1$, $J=5.5 \leftarrow 4.5$, $F_1=7 \leftarrow 6$ Center frequency: 197268.8470 MHz. For CMB v=4 (bottom right): $N=8 \leftarrow 7$, $K=1 \leftarrow -1$, $J=8.5 \leftarrow 7.5$, $F_1=9 \leftarrow 8$ Center frequency: 303629.23460 MHz For All: Span frequency: 1 MHz Averaged # of Sweeps: 120 # of Steps: 50 Scan increments: 0.02 MHz.

III.C. Discussion on the $O(^1D) + X$ Reactions

While we have not seen product signal for the $O(^1D) + X$ reaction, we feel confident that our setup and detection method is conducive for product formation and detection. With that said, for future experiments with the $O(^1D) + X$ reaction, we may choose to stick with SMB conditions until product signal is found, in the hopes that the collisions within the molecular beam will slow down the $O(^1D)$ atom, and thereby increasing its collisional cross section and the likelihood of product formation.

Even though we switch to the $O(^1D) + CHCl_3$ experiment because we had rotational data on the ClO product up to the $v=7$ state we have yet to find signal. It is possible that the $O(^1D) + CHCl_3$ reaction is preferentially producing HCl and so in future experiments we plan on switching to carbon tetrachloride (CCl_4) or Chlorine gas (Cl_2) as our chlorine source. These gases also have a more favorable rate constant with $O(^1D)$.

III.D. Conclusions

This thesis describes a set of experiments with the goal of measuring product rovibronic state distributions of bimolecular reactions by direct mm-wave absorption under both crossed molecular beam and single molecular beam conditions. The work attempted to detect the formation of XO ($X = Br, I, Cl$) products from the reactions $X + O_3$ ($X = I$ and Br) and $O(^1D) + X$ ($X = Br_2, I_2, N_2O$, and $CHCl_3$). If successful, it would have added high resolution detail to prior crossed molecular beam studies of these systems. While no product signals have been observed to date, the thesis outlines some of the experimental pitfalls along the way. We have systematically chosen systems with

increasingly large reaction cross sections in the hopes of obtaining signal. On the experimental side, it is possible that by decreasing sources of noise, optimizing laser and millimeter wave overlap and/or by using multipass configurations and longer averaging products may eventually be detected and optimized. It is also possible that the product state distributions are simply too broad-peaked at an inaccessibly high rotational states, or they are in vibrational or electronic states for which we have no transition frequencies.

On the experimental side, the delivery of non-gaseous reagents to the chamber has proved successful for liquids (bromine and chloroform). However, for solid reagents, like iodine, external delivery systems proved ineffective. A solution to this would be to heat the entire external system.

Back-flow of exhaust gases between nozzles has proved problematic in obtaining clean CMB signals. A solution to this problem would be to design nozzle arms that prevent the flow of gases between each other. The Duffy lab has recently gained access to a 3D printer, so the arms could be designed and made out of plastic on site, allowing us to tweak the arm design as needed.

Successful diagnostic scans have been developed and tested, which allows us to optimize and identify experimental issues before running experiments. Future work in testing the product distribution of ClO from CMB and SMB experiments may prove more successful with the use of chlorine gas, or carbon tetrachloride. Once a successful ClO signal has been obtained, we can use those experimental conditions to try and detect BrO or IO.

REFERENCES

- [1] The Noble Prize in Chemistry 1995. Nobleprize.org. Noble Media AB 2013. Web. http://www.nobleprize.org/noble_prize/chemistry/laureates/1995/ Accessed: September 22, 2013.
- [2] Speth, J.G. 2004. *Red Sky at Morning: America and the Crisis of the Global Environment* New Haven: Yale University Press, pp. 95.
- [3] Class I Ozone Depleting Substances. Epa.gov. Web. <http://www.epa.gov/ozone/science/ods/classone.html> Accessed: September 4, 2013.
- [4] Zhang, J.S.; Lee, Y.T. J. Phys. Chem. 1997, 101, 6485-6495.
- [5] Bell, N.; Hsu, L.; Jacob, D.J.; Schultz, M.G.; Blake, D.R.; Butler, J.H.; King, D.B.; Lobert, J.M.; Maier-Reimer, E. J. Geophys. Res.: Atmos., 2002, 107, 4340.
- [6] NOAA Study Shows Nitrous Oxide Now Top Ozone-Depleting Emission. Noaa.gov. Linda Joy. Web. http://www.noaanews.noaa.gov/stories2009/20090827_ozone.html Accessed: June 30, 2014.
- [7] NOAA Study Shows Nitrous Oxide Now Top Ozone-Depleting Emission. Noaa.gov. Linda Joy. Web. http://www.noaanews.noaa.gov/stories2009/20090827_ozone.html Accessed: June 30, 2014.
- [8] NIST Chemical Kinetics Database Cl + O₃. Nist.gov. Web. <http://www.kinetics.nist.gov/kinetics/Search.jsp> Accessed: September 4, 2013.
- [9] Miller, W.B.; Safron, S.A.; Herschbach, D.R. Discuss. Faraday Soc. 1979, 67, 27.

- [10] McGrath, W.P.; Norrish, R.G.W.Z. *Phys. Chem. (Munich)* 1958, 15, 245.
- [11] Molina, L.T.; Molina, M.J.; *J. Phys. Chem.* 1987, 91, 433.
- [12] McElroy, M.B.; Salawitch, R.J.; Wofsy, S.C.; Logan, J.A. *Nature* 1986, 321, 759.
- [13] Zhang, J.S.; Miao, T.T.; Lee, Y.T. *J. Phys. Chem. A.* 1997, 101, 6922-6930.
- [14] Solomon, S.; Garcia, R.R.; Ravishankara, A.R.; *J. Geophys. Res.* 1994, 99, 20491.
- [15] Tucceri, M.E.; Dillon, T.J.; Crowley, J.N.; *Phys. Chem. Chem. Phys.* 2005, 7, 1657-1663.
- [16] D. Holscher, C. Fockenberg and R. Zellner, *Ber. Bunsen-Ges. Phys. Chem.*, 1998, 102, 716–722.
- [17] Hay, P.J.; Pack, R.T.; Walker, R.B.; Heller, E.J. *J. Phys. Chem.* 86, 1982, 862-865.
- [18] Finlayson-Pitts, B.J.; Pitts, J.N. *Atmospheric Chemistry* Wiley, New York 1986.
- [19] Munson, M.S.B. *J. Am. Chem. Soc.*, 1965, 87, 5313.
- [20] MacNeil, K.G.; Futrell, J.H. *J. Phys. Chem.* 1972, 76, 409.
- [21] Kauczok, S; Maul, C.; Chichinin, A.I.; Gericke, K.H. *J. Chem. Phys.* 2010, 132, 244308.
- [22] Monge, Josue R. *Constructing Velocity Distributions in Crossed-Molecular Beam Studies Using Fourier Transform Doppler Spectroscopy*. Greensboro, N.C: University of North Carolina at Greensboro, 2012. Internet resource.
- [23] Kinsey, J.L. *J. Chem. Phys.*, 1977, 66, 2560-2565.
- [24] Mark, Nicholas R. *A New Crossed Molecular Beam Apparatus for the Study of the Cl + O3 Reaction Probed Via Direct Absorption of Millimeter/submillimeter-Waves*. Greensboro, N.C: University of North Carolina at Greensboro, 2012. Internet resource.

- [25] Ren,Z.; Qiu, M.; Che, L.; Dai, D.; Wang, X.; Yang, X. *Rev. Sci. Inst.* 77, 2006, 016102.
- [26] Mauney, Daniel T. *New Instrument for Probing the Pure Rotational Spectroscopy of Cold Molecules Produced Via "billiard-Like" Scattering*. Greensboro, N.C: University of North Carolina at Greensboro, 2012. Internet resource.
- [27] Ozone Decomposition.
<http://www.lenntech.com/library/ozone/decomposition/ozone-decomposition.htm>
Accessed: September 3, 2013.
- [28] Mordecai, R.B. *Bull. Hist. Chem.*, 2008, 33, 68-75.
- [29] MSDS Ozone (Ambient Air Gas). mcpur.com, Mar Cor Purification,
http://www.mcpur.com/main/library/msds/MSDS_Ozone_ME80675e.pdf Accessed: July 25, 2014. Internet resource.
- [30] Smedly, J.E.; Haugen, H.K.; Leone, S.R. *J. Chem. Phys.* 87, 1987, 5, 2700-2708.
- [31] Atkinson, R.;Baulch, D.L.;Cox, R.A.;Crowley, J.N.;Hampson, R.F.;Hynes, R.G.;Jenkin, M.E.;Rossi, M.J.;Troe, J. *Atmos. Chem. Phys.* 7, 2007, 981-1191.
- [32] Atkinson, R.; Baulch, D.L.; Cox, R.A.; Hampson Jr., R.F.; Kerr, J.A.; Troe, J. *Phys. Chem. Ref. Data* 18, 1989, 881-1097.
- [33] Steinfeld, J.; Francisco, J.; Hase, W. *Chemical Kinetics and Dynamics*. Prentice Hall, 1989, 247.
- [34] Tokel, O.; Chen, J.; Ulrich, C. K.; Houston, P. L. *J. Phys. Chem. A* 2010, 114, 11292-11297.

[35] Mandin, J.Y.; Dana, V.; Regalia, L.; Barbe, A.; Thomas, X. *J. Mol. Spec.* 1997, 185, 347-355.